Geochemistry, Geophysics, Geosystems®

RESEARCH ARTICLE
10.1029/2022GC010838

Key Points:

- Extensive CO_2 soil degassing measurements and carbon isotopic composition in the Larderello geothermal system were carried out
- Hydrothermalized hot- and cold-degassing areas are controlled by structural setting
- Regional transfer zones enhance the circulation of deep-seated geothermal fluids

Supporting Information:

Supporting Information may be found in the online version of this article.

Correspondence to:

M. Taussi,
marco.taussi@uniurb.it

Citation:

Taussi, M., Nisi, B., Brogi, A., Liotta, D., Zucchi, M., Venturi, S., et al. (2023). Deep regional fluid pathways in an extensional setting: The role of transfer zones in the hot and cold degassing areas of the Larderello geothermal system (Northern Apennines, Italy). *Geochemistry, Geophysics, Geosystems*, *24*, e2022GC010838. https://doi.org/10.1029/2022GC010838

Received 20 DEC 2022
Accepted 15 APR 2023

Deep Regional Fluid Pathways in an Extensional Setting: The Role of Transfer Zones in the Hot and Cold Degassing Areas of the Larderello Geothermal System (Northern Apennines, Italy)

Marco Taussi[1], Barbara Nisi[2], Andrea Brogi[3,4], Domenico Liotta[3,4], Martina Zucchi[3], Stefania Venturi[2,5], Jacopo Cabassi[2], Gabriele Boschi[5], Marika Ciliberti[6], and Orlando Vaselli[2,5]

[1]Dipartimento di Scienze Pure e Applicate, Università degli Studi di Urbino Carlo Bo, Urbino, Italy, [2]CNR-IGG Istituto di Geoscienze e Georisorse, Consiglio Nazionale delle Ricerche, Firenze, Italy, [3]Dipartimento di Scienze della Terra e Geoambientali, Università degli Studi di Bari Aldo Moro, Bari, Italy, [4]CNR-IGG Istituto di Geoscienze e Georisorse, Consiglio Nazionale delle Ricerche, Pisa, Italy, [5]Dipartimento di Scienze della Terra, Università di Firenze, Firenze, Italy, [6]Deda Next Srl, Borgo Panigale Bologna, Italy

Abstract High-temperature geothermal areas are often characterized by widespread surficial manifestations, whose location is strictly controlled by sets of faults of regional relevance. The geochemical and isotopic signature of the discharged fluids can reveal key information on the geothermal fluids pathway, shedding light on the sources and fluid-rock interaction within the geothermal reservoirs. In this paper, a geochemical and structural data set from the Larderello geothermal area and surroundings is presented and discussed. We constrain the role of transfer and normal faults in controlling the geothermal circulation enhanced by a cooling magmatic intrusion underneath the Lago area (SW of Larderello). The structural control on the fluids circulation is highlighted by both the location of the CO_2 emissions along the fault segments, where permeability is enhanced, and their degassing rates, which increase moving away from the core of the Larderello geothermal system. The main results unravel the presence of deep regional pathways along which endogenous fluids circulate before being discharged in the investigated areas. The peripheral zone emissions are affected by interaction with shallow aquifers and condensation processes whereas the CO_2 emitted from the central areas, located near the core of the geothermal system, was accompanied by high amounts of steam, and suffers intense shallow fractionation processes. The latter areas emit medium-to-low normalized-CO_2-degassing rates (<270 t d^{-1} km^{-2}) when compared to the extremely high values occurring in the peripheral sectors (up to 1,300 t d^{-1} km^{-2}) of the Larderello geothermal systems, possibly suggesting an incipient propagation of such a system, likely wider than previously thought.

Plain Language Summary High-temperature geothermal areas are specific zones on Earth where the geothermal gradient is greater than the average global value (~30°C km^{-1}). This is due to the existence of cooling magma source(s) at depth, providing heat that is transmitted to fluid reservoir(s) located at intermediate levels continuously and naturally fed by recharging fluids, and sealing rock(s) at shallower levels that maintain reservoir temperature and pressure. These geothermal areas commonly show steam-dominated manifestations at the surface, accompanied by relevant degassing of carbon dioxide likely originated from different feeding systems (biogenic, thermometamorphic, and mantellic). Defining sources, processes, and transport mechanisms governing the CO_2 emissions from soils is challenging but pivotal to understand the geothermal fluid origin, dynamics, and relation with the geological structures. To unravel these processes, we combined geochemical and structural measurements performed at the Larderello-Travale-Radicondoli (LTR) geothermal field (Italy). Distinct geothermal sectors were investigated according to their geochemical characteristics, CO_2 degassing rates, and geological-structural features, to understand how CO_2 is transported and modified during its journey from the deep geothermal reservoir(s) to the surface, exploiting the permeability of fault zones and/or fractured rocks. Results suggest that the LTR geothermal system might be wider than previously thought, indicating a higher geothermal potential.

1. Introduction

Independently by their magmatic/metamorphic and/or meteoric origin, upflow of hydrothermal fluids is favored by the increased permeability of rocks. This is caused by fracture networks related to regional fault zones which can affect significant crustal volumes (Anderson & Fairley, 2008; Caine et al., 1996; Curewitz & Karson, 1997;

Ganerød et al., 2008; Sibson, 2000). The permeability of fault damage zones depends on fault kinematics since the most favorable direction of a fluid flow corresponds to the attitude of the intermediate axis of the local active stress field (Faulkner & Armitage, 2013; Faulkner et al., 2010; Sibson, 2000). As a consequence, following the Andersonian theory, the damage zone of strike-slip to oblique-slip faults is suitable to channel deep fluids from depth to shallow levels, being the intermediate stress axis vertical or close to it (e.g., Rowland & Sibson, 2004). For the same reason, damage zones of normal faults are expected to favor the lateral migration of fluids (Sibson, 2000). Moreover, strike- and oblique-slip faults, and normal faults can coexist within the same regional stress field, when the former play the role of transfer faults. In this case, transfer faults are almost orthogonal to the normal faults' orientation and parallel to the main direction of crustal stretching (Bally, 1981; Faulds & Varga, 1998; Gibbs, 1984).

Transfer faults are combined to form transfer zones affecting km-wide crustal volumes (Van der Pluijm & Marshak, 1996). Transfer zones are characterized by parallel and/or anastomosed fault segments (i.e., the transfer faults) at high-angle to the regional trend of the rift (Brogi et al., 2020; Liotta & Brogi, 2020), which accommodate the heterogeneous extension, splitting the crust into domains with different amounts of extension (Gibbs, 1990) and favoring the development of independent tectonic depressions (Alçiçek et al., 2013, 2018; Martini & Sagri, 1993). The orientation of the transfer zones and their propagation into the deeper crustal levels might be inherited by pre-existing crustal-scale structures (Liotta, 1991), thus favoring the development of permeable rock-volumes that constitute preferential pathways for deep fluids. In such a context, fluid circulation is promoted by the hydraulic connectivity between the dominantly vertical and horizontal pathways related to strike-slip to oblique-slip and normal faults, respectively (Cox et al., 2001; Faulds et al., 2012; Liotta et al., 2021; Olvera-Garcia et al., 2020; Sillitoe & Brogi, 2021).

The northern Tyrrhenian Sea (Bartole, 1995) and southern Tuscany (Martini & Sagri, 1993) are excellent examples of the coexistence between transfer and normal fault systems, active since the Miocene (Acocella & Funiciello, 2006; Bartole, 1995; Brogi & Liotta, 2008; Liotta, 1991). Then, the diffuse hydrothermal mineralization characterizing the area (Tanelli, 1983), triggered by crustal magmatism (Dini et al., 2005; Serri et al., 1993), accounts for the continuous development of geothermal systems during ongoing extension. However, the detection of the structures associated with transfer zones (and related fluid circulation) can result problematic if regional uplift and weathering occurred, the latter determining fluvial incisions and valleys developing along fault traces (Rossello & Gallardo, 2022), or if almost homogeneous sedimentation developed within the minor structural depressions associated with the regional transfer zones (e.g., Brogi et al., 2013). This is the case of southern Tuscany, where the progressive uplift induced by extensional tectonics (Dallmeyer & Liotta, 1998) has produced incised valleys strictly controlled by faults (including the regional transfer zones), thus masking the fault traces at the ground surface.

In this framework, an excellent contribution to detect fault traces is given by both the location of the geothermal manifestations (e.g., Liotta et al., 2021) and the isotopic signature of CO_2 emissions, which can reveal much on their origin. In fact, deeply sourced CO_2 (metamorphic and/or magmatic in origin) is usually degassed along discrete pathways, rather than degassed evenly throughout a larger volcanic or hydrothermal area (Rahilly & Fischer, 2021). The variations in terms of CO_2 fluxes can be large, thus a reliable way to estimate these emissions from hidden faults is through high density and spatially extensive measurement points employing the accumulation chamber method (e.g., Camarda et al., 2019; Chiodini et al., 1998).

This approach was applied to the transfer zone along which the Larderello geothermal system is developing (Liotta & Brogi, 2020), with a twofold goal. The first is to compute a first quantification of the diffuse CO_2 flux emitted from one of the most famous geothermal fields in the world by incorporating measurements from both thermally active and cold degassing (hydrothermally altered) soils located near the core and at the periphery of the geothermal system, respectively. The second is to bring further elements to define the role of the transfer zones in controlling the geothermal fluid pathways. Carbon dioxide fluxes and carbon isotopic composition of CO_2 in the interstitial soil gas were therefore measured in several areas within the Larderello geothermal field to identify the origin of the CO_2 and its link with the geothermal reservoir(s), also estimating the shallow (biogenic) and deep (endogenous) contributions to the total CO_2 emission from the study geothermal system.

2. Geological and Geothermal Setting

2.1. Geological Background

The Larderello geothermal system is located in the inner Northern Apennines, a NE-verging Alpine belt deriving from the convergence and collision (Cretaceous-early Miocene) of the Adria and European continental margins (Vai & Martini, 2001). The collision produced HP-metamorphism (up to 1.5 GPa) related to the eastward stacking of the tectonic units of oceanic and continental pertinence (Bianco et al., 2015, 2019; Brogi & Giorgetti, 2012; Brunet et al., 2000; Giuntoli & Viola, 2021; Rossetti et al., 2002). Since the early Miocene, the orogenic belt was (and still is) affected by eastward propagating extensional tectonics (Barchi, 2010; Brogi, 2020; Carmignani et al., 1995), which caused (a) Miocene lateral segmentation of the previously stacked units (e.g., Brogi & Liotta, 2008; Carmignani et al., 2001); (b) development of NW-striking Pliocene-Quaternary normal faults, dissecting previous structures and forming tectonic depressions filled by continental and marine sediments (Martini & Sagri, 1993). The primary effects of crustal and lithospheric-scale extensional tectonics were the opening of the Tyrrhenian Basin (Bartole, 1995), the present-day crustal and lithospheric thickness of about 22 and 40 km, respectively (Calcagnile & Panza, 1981; Di Stefano et al., 2011), and the widespread anatectic and subcrustal magmatism developed since the Langhian (Serri et al., 1993; Smith et al., 2011). Magmatism favored the emplacement of felsic intrusions at shallow crustal levels (<8 km depth; Serri et al., 1993) mostly along the NE-striking transfer zones (Brogi et al., 2021; Dini et al., 2008; Liotta et al., 2015; Spiess et al., 2021) that roughly follow the orientation of the minimum compressional axis, as reconstructed from breakout analysis (Mariucci et al., 1999; Mariucci & Montone, 2020). In Tuscany (i.e., inner Northern Apennines), the emplacement of magmatic bodies at the shallow crustal levels produced widespread meso- and epithermal base ore deposits, exploited for centuries (Tanelli, 1983). The present diffuse geothermal anomaly has an average heat flux value of 120 mW m^{-2} and local peaks up to 1,000 mW m^{-2}, as estimated in the Larderello geothermal system area (Della Vedova et al., 2001).

The Larderello system consists of different geothermal fields. Considering the highest geothermal gradient (exceeding 100°C km^{-1}; Batini et al., 2003), the most significant is located in the Lago Basin (Figure 1), from where the bulk of electricity production derives (Barbier, 2002). The heat source of the geothermal anomaly is thought to be related to a cooling magmatic body at shallow depths (3–6 km) below the Lago Basin, as suggested by teleseismic data analyses (Foley et al., 1992), interpretation of deep reflection seismic lines (Accaino et al., 2005; Brogi et al., 2005), magnetotelluric studies (Manzella, 2004) and rheological models (Rochira et al., 2018). The tectonic and stratigraphic units occurring in the whole Larderello geothermal area have been described by many authors, based on fieldwork (e.g., Costantini et al., 2002; Lazzarotto, 1967; Lazzarotto & Mazzanti, 1978; Liotta & Brogi, 2020) and borehole logs (e.g., Bertini et al., 2006; Dini et al., 2005; Elter & Pandeli, 1990; Pandeli et al., 1991, 1994; Romagnoli et al., 2010). Figure 1 shows the updated geological map of the Larderello geothermal area, where the main Neogene-Quaternary normal and transfer faults are reported.

Information on the deeper structural levels (Figure 2) derives from the interpretation of reflection seismic lines, displaying the occurrence of a high-impedance seismic reflector, known as the K-horizon (Batini et al., 1978; Cameli et al., 1993). This reflector, ranging in depth between 3 and 6 km, is believed to derive from high-pressure fluids, entrapped in a fractured active shear zone (Batini et al., 1983) located at the top of the brittle-ductile transition (Cameli et al., 1993, 1998; De Matteis et al., 2008; Liotta & Ranalli, 1999), where fluids in supercritical conditions (Agostinetti et al., 2017; de Franco et al., 2019; Romagnoli et al., 2010) are inferred. The K-horizon in the Larderello area shows a dome-shaped geometry with its culmination in correspondence of the Lago Basin depocenter (e.g., Brogi et al., 2005), where the highest values of heat flux (up to 1,000 mW m^{-2}; Della Vedova et al., 2001) and $^{3}He/^{4}He$ isotopic ratios (up to 3.2 Ra; Magro et al., 2003) were measured, suggesting that the Lago Basin is a preferential area for the escape of mantle-derived fluids (Magro et al., 2003). In this framework, the local seismicity (http://cnt.rm.ingv.it) indicates a continuous process of active deformation, thus permitting the permeability maintenance and promoting the positive loop triggering fluid-pressure and fractures.

2.2. Geothermal Background

That of Larderello is the oldest exploited geothermal system in the world for electricity purposes (Batini et al., 2003; Romagnoli et al., 2010), with a nowadays-installed capacity of more than 790 MWe (Manzella et al., 2018). It is one of the few steam-dominated geothermal systems in the world, which evolved from an initially liquid state to its current superheated steam condition thanks to the thermal and structural setting (Gola et al., 2017; Romagnoli

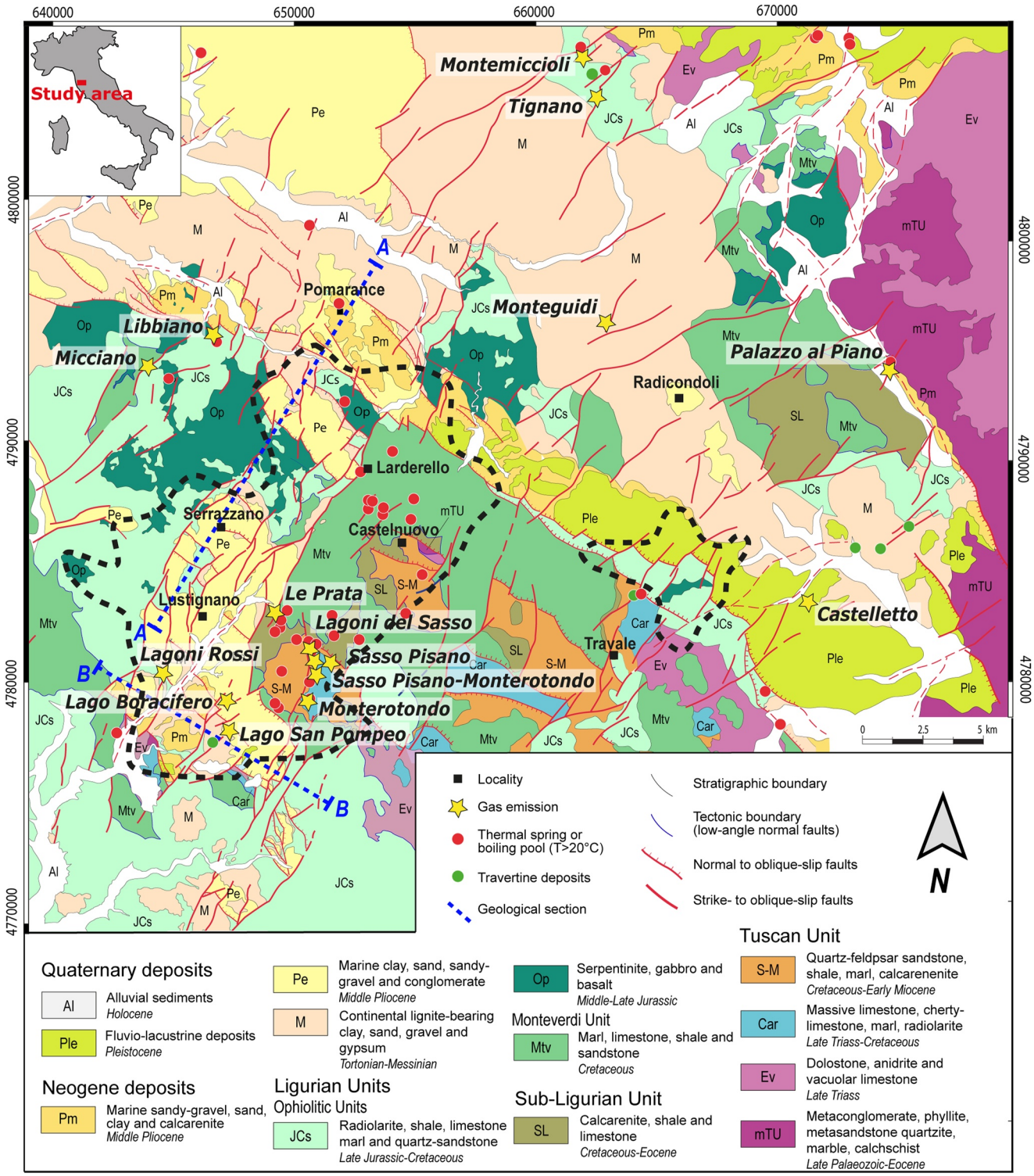

Figure 1. Geological map of the Larderello geothermal area (modified after Liotta & Brogi, 2020) where the main geothermal manifestations are indicated. Location of gas emissions, thermal springs, and travertine deposits are from this work, Minissale (2004), geothopica (www.geothopica.igg.cnr.it), and maga databases (www.magadb.net). The black dashed lines circumscribe the location of most of the geothermal wells (after www.geothopica.igg.cnr.it). Blue dashed lines indicate the geological cross sections reported in Figure 2.

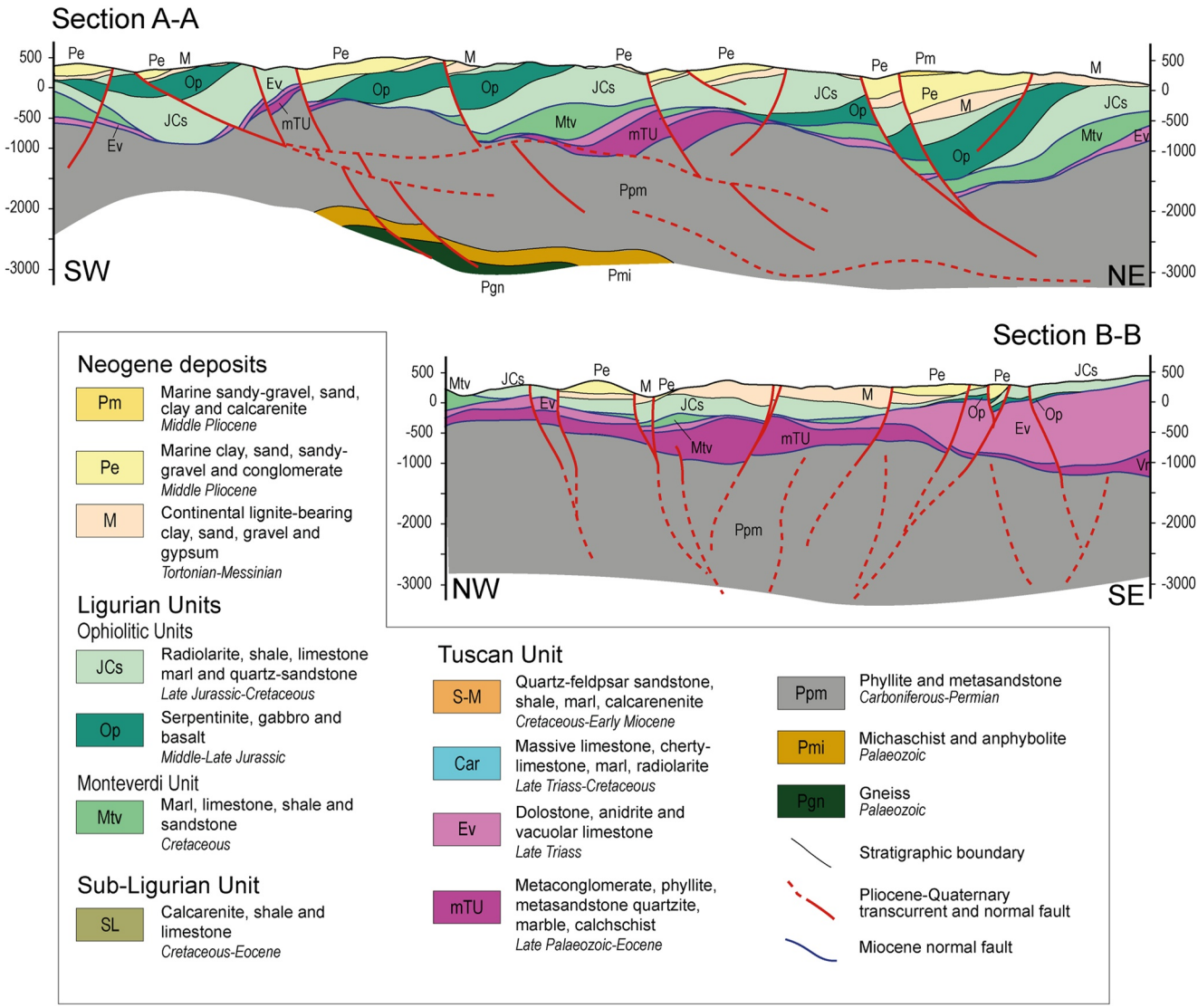

Figure 2. Geological cross sections through the study area (Figure 1), modified from Liotta and Brogi (2020).

et al., 2010). The liquid phase is presently confined to a few local structures that facilitate the seepage of meteoric waters into the reservoir due to the presence of permeable carbonate outcrops (Gola et al., 2017). The field, which comprises the areas of Larderello, Travale and Radicondoli (Figure 1), covers a surface area of ~120 km^2 (Bertani et al., 2005; Romagnoli et al., 2010) and is characterized by two geothermal reservoirs used for power production, confined above by the presence of about 1,000 m thick nearly impermeable formations which act as a cap-rock (Miocene-Pliocene clayey and sandy sediments and Cretaceous-Oligocene marly Flysch Units; e.g., Batini et al., 2003). The shallow (500–1,500 m b.g.l.) and deep (1,900–4,000 m b.g.l.) reservoirs are hosted in the Mesozoic carbonate-anhydrite formations of the Tuscan Nappe and in the Palaeozoic metamorphic successions, respectively, having temperatures of 150°C–250°C and >300°C, respectively (e.g., Batini et al., 2003; Bertani et al., 1999; Bertini et al., 2006; Bolognesi, 2011; Gianelli et al., 1997; Romagnoli et al., 2010).

Water composition in the liquid-dominated parts of the field is highly variable ranging from NaCl and $NaHCO_3$ in the north-western sector (Minissale, 1991; Panichi et al., 1974) to $CaSO_4$ in the south-eastern one (Ceccarelli et al., 1985), depending on the different water-rock interaction after steam condensation (Duchi et al., 1992; Minissale, 1991). The geothermal steam is mainly consisting of H_2O (>90%), CO_2, CH_4, H_2S, H_2, and N_2, with noble gases at ppm levels (Gherardi et al., 2005; Magro et al., 2003; Minissale et al., 1997; Scandiffio et al., 1995). Oxygen and hydrogen stable isotope data on H_2O indicate meteoric water as the main source of the vapor (Craig, 1963; Ferrara et al., 1965), with a minor contribution from shallow perched aquifers (Romagnoli

et al., 2010). Carbon dioxide at Larderello is about 3–10 wt.% of the total fluid composition (D'Amore & Truesdell, 1984; Bertini et al., 2006) and is produced by thermo-metamorphic processes also supplied by magmatic (mantle-derived) contributions (Gherardi et al., 2005; Gianelli et al., 1997), as suggested by the $\delta^{13}C\text{-}CO_2$ values ranging from −7.1‰ to −1.4‰ versus V-PDB (Gherardi et al., 2005). The magmatic contribution is also supported by the $^3He/^4He$ ratios, which range from 0.5 up to 3.2 Ra measured in both, geothermal wells and surface manifestations (Hooker et al., 1985; Magro et al., 2003; Minissale, 2004; Minissale et al., 1997).

3. Materials and Methods

3.1. CO_2 Flux, Interstitial Soil Gas and Temperature Measurements

A total amount of 648 CO_2 flux measurements was carried out in nine different areas of the Larderello geothermal field and neighboring zones (Figure 3), following the accumulation chamber method (e.g., Cardellini et al., 2003; Chiodini et al., 1998; Jentsch et al., 2020). In specific degassing areas, interstitial gas samples (n.77) for the determination of the $\delta^{13}C\text{-}CO_2$ values (expressed as ‰ vs. V-PDB—Vienna-Pee Dee Belemnite) were collected. In the Monterotondo Marittimo area (hereafter Monterotondo) previously published data by Venturi et al. (2019) and Cabassi et al. (2021), consisting of 35 interstitial CO_2 carbon isotopic composition and 89 measurements of CO_2 flux, respectively, carried out in the area named Monterotondo-S (Figure 3b) were also taken into account.

The investigated areas represent most of the numerous degassing zones related to the Larderello geothermal system (Figure 1). Security, danger, and access issues prevented any survey in other degassing sites. Surveyed areas were carried out during different years and seasons, always with stable meteorological conditions and away (at least 1 week) from heavy rains. They were completed in a few hours, depending on the extension of each area, to avoid major atmospheric changes that could have affected the soil flux measurements (e.g., Lelli & Raco, 2017). Specifically, most surveys were carried out in summer (Monterotondo-N, Monterotondo-S, Lagoni-Sasso, Micciano-NW, Libbiano, Palazzo al Piano and Montemiccioli), while two areas were investigated in autumn (Sasso Pisano and Sasso-Monterotondo) and one in winter (Micciano-SE). The main features and sampling details of each surveyed area are reported in Table 1. Field photographs of the investigated areas are reported in Supporting Information S1.

The portable fluxmeter used in this work has a detection limit of ∼0.08 g m^{-2} day^{-1} (https://www.westsystem.eu/it) and was calibrated at the manufacturing company (West Systems) before each fieldwork through calibration curves (Tassi et al., 2016). The equipment consists of a type A cylindrical metal vessel (the accumulation chamber) positioned on the ground avoiding rugged morphology to prevent the ingression of air, a Licor Li-820 Infra-Red (IR) spectrophotometer, an analogical-digital converter, and a palmtop computer. The accumulation chamber had a volume of ∼2.8 L and was equipped with a ring-shaped perforated collector to re-inject the circulating gas through a low-flow pump (20 mL s^{-1}), thus guaranteeing the mixing of the soil gas into the chamber which was also favored by a rotating fan. The spectrophotometer detector had a sensor operating in the range of 0–20,000 ppm of CO_2 (accuracy: 4%). The soil gas circulated from the chamber to the IR sensor and vice versa via a pump (∼1 L min^{-1}) and the signal was converted by an analogical-digital converter and transmitted to the palmtop computer, where a CO_2 concentration versus time diagram was plotted in real-time. Next to each soil CO_2 sampling point, marked with a portable GPS Garmin GPSmap 62st and by reference points in the field, soil temperatures were measured using a TERSID thermocouple (dynamic range from −20°C to 1,150°C; uncertainty ±0.1°C; Tassi et al., 2016) inserted into the soil for a couple of centimeters to avoid wind influence. The spatial distribution and the density of the measurement spots were influenced by rocky, irregular, impervious, and steep grounds and, in some cases, by the presence of dense Mediterranean vegetation (Table 1). Diffuse soil gas measurements close to the fumaroles were avoided to prevent a large amount of steam and dust from entering the IR sensor, although Mg-perchlorate and cellulose nitrate filters were installed.

Interstitial soil gas samples for C-isotopic analyses were collected with a 4 mm inner-diameter stainless-steel tube inserted at ∼20 cm depth from selected areas of low, intermediate, and high soil CO_2 flux. The tube was connected, through a silicone tube and PTFE three-way valve, to a 60 mL plastic syringe. The latter allowed to rinse the whole geometry and pump the soil gas to a 12 mL glass vial equipped with a pierceable rubber septum (Labco Exetainer®) for isotopic analyses by using the double-needle method (e.g., Tassi et al., 2015; Venturi et al., 2019).

3.2. Analytical Methods

The carbon isotopic composition of carbon dioxide ($\delta^{13}C\text{-}CO_2$ expressed as ‰ vs. V-PDB) was analyzed by Cavity Ring-Down Spectroscopy (CRDS) using a Picarro G2201-i Analyzer following the procedure described by Venturi et al. (2019). The instrument inlet line was equipped with a Drierite trap and a copper trap to avoid

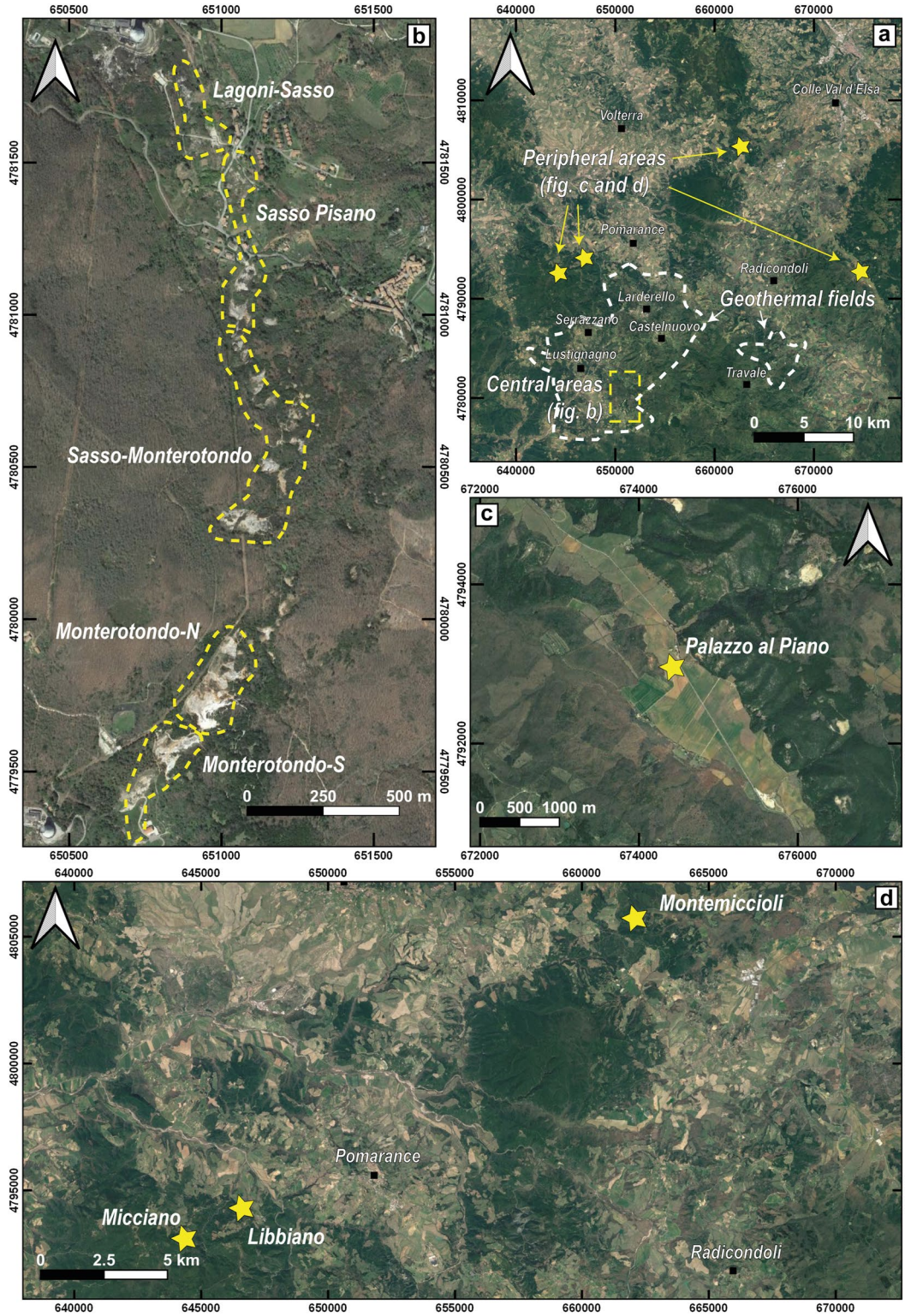

Figure 3. Locations of the sampled areas. (a) General view of central and peripheral areas with (b) detail of the central areas division, and (c–d) of the peripheral areas.

Table 1
Sampling Location and Date, Number of the CO_2 Flux and $\delta^{13}C$-CO_2 in the Interstitial Gas Measurements and Surface of Each Surveyed Area

Site	Date	N. points		Surveyed area (m^2)	Soil type	Vegetation	Figures
		CO_2 flux	Isotopic samples				
				Central areas			
Monterotondo-N	September 2019	98	18	27,117	Highly fractured and hydrothermally altered rocks with scattered loosy soils	Woodland and Mediterranean bush	Figure S1 in Supporting Information S1
Monterotondo-S[a]	August 2017	89	35	20,000	Highly fractured and hydrothermally altered rocks with scattered loosy soils	Woodland and Mediterranean bush	Figure S1 in Supporting Information S1
Sasso-Monterotondo	November 2019	75	3	20,237	Rocky and hydrothermally altered soils	Mediterranean bush	Figure S5 in Supporting Information S1
Sasso Pisano	October 2019	41	8	10,128	Rocky and hydrothermally altered soils	Mediterranean bush	Figure S5 in Supporting Information S1
Lagoni-Sasso	September 2020	75	-	8,550	Rocky and hydrothermally altered soils	Mediterranean bush	Figure S9 in Supporting Information S1
Total		378	64	86,032			
				Peripheral areas			
Micciano-NW	August 2019	64	–	2,610	Rocky and hydrothermally altered soils	Woodland, Mediterranean bush and sporadic rushes	Figure S13 in Supporting Information S1
Micciano-SE	February 2020	49	–	2,770	Rocky and hydrothermally altered soils	Woodland and Mediterranean bush	Figure S17 in Supporting Information S1
Libbiano	July 2018	52	23	1,945	Rocky and hydrothermally altered soils	Woodland, Mediterranean bush, and arable field	Figure S21 in Supporting Information S1
Palazzo al Piano	August 2019	82	8	30,920	Clayey soils	Arable field	Figure S25 in Supporting Information S1
Montemiccioli	July 2017	112	17	14,970	Rocky and hydrothermally altered soils	Woodland	Figure S29 in Supporting Information S1
Total		359	48	53,215			
Total		737	112	139,247			

[a]Data from Venturi et al. (2019) and Cabassi et al. (2021).

interferences and remove water vapor and H_2S, respectively. Due to the operative ranges of the Picarro G2201-i Analyzer, gas samples showing CO_2 concentrations higher than 2,000 ppmV were diluted with high-purity chromatographic air. Internal standards consisting of CO_2 (Air Liquide), with $\delta^{13}C$-CO_2 of −28‰ versus V-PDB and −5.2‰ versus V-PDB, respectively, were used to calibrate and test the reproducibility of the Picarro measurements. The analytical error for $\delta^{13}C$-CO_2 was ±0.16‰.

3.3. Data Processing and CO_2 Output Estimation

The statistical distributions of the soil CO_2 fluxes were processed by using the Graphical Statistical Analysis (GSA) method (Chiodini et al., 1998), performed according to the procedure proposed by Sinclair (1974). This method consists of plotting individual flux points on a cumulative log-probability diagram, evaluating the eventual inflection point(s) which determines the number of discrete populations and their proportion. The

GSA approach and the isotopic content of the interstitial gas were used to characterize the source(s) of the discharged CO_2 at ground level. Kriged distribution maps of the soil CO_2 flux were created using the ISATIS© software package of Geovariances and then graphically reported using the QGIS software. It is worth noting that the inhomogeneous distribution of the measurement points caused by the rough morphology of the sites prevented the possibility of obtaining a regular grid, which inevitably affected the semivariogram construction. The semivariograms, the cross-validation diagrams, and the standard deviation maps of the studied areas are reported in Figures S2–S4, S6–S8, S10–S12, S14–S16, S18–S20, S22–S24, S26–S28, and S30–S32 in Supporting Information S1.

The total CO_2 output of each investigated area was calculated by applying Sichel's t-estimator (Mi) (David, 1977). The estimated CO_2 output was derived by multiplying M_i times the area covered by each estimated population. In the same way, the central 95% confidence intervals of the CO_2 output were used to calculate the uncertainty of each population. Where the presence of outliers was recognized, their contribution was added, considering the flux over the basal area of the accumulation chamber (i.e., 0.0308 m^2).

4. Results

4.1. Soil CO_2 Flux and Temperature, and Isotopic Composition of the Interstitial Gases

The main statistical parameters of each soil CO_2 population recognized in every area, along with the $\delta^{13}C$-CO_2 isotopic composition in the interstitial gas, are summarized in Table 2. Information on the data set containing coordinates, soil temperature, atmospheric pressure, soil CO_2 flux data, and $\delta^{13}C$-CO_2 values for each measurement point are reported in Taussi et al. (2023).

4.1.1. Central Areas

Among the five central areas of Larderello (Monterotondo-N, Monterotondo-S, Sasso-Monterotondo, Sasso Pisano, and Lagoni-Sasso; Figure 3b), the soil CO_2 fluxes were ranging from 0.2 to 3,338 g m^{-2} day^{-1}, except for Monterotondo-N where the two highest values were recorded that is, 21,077 and 29,838 g m^{-2} day^{-1} (Table 2). From a general point of view, the mean values of the entire data sets in the central areas varied from 41 (Lagoni-Sasso) to 795 g m^{-2} day^{-1} (Monterotondo-N), whereas for the other investigated zones (Monterotondo-S, Sasso Pisano, Sasso-Monterotondo) the CO_2 flux was ranging between ~118 and ~201 g m^{-2} day^{-1}. The $\delta^{13}C$-CO_2 values of the interstitial gas sampled from Monterotondo-N and Monterotondo-S stretched over a wide range, from −26.3 up to +3.5‰ versus V-PDB, with a mean value of −4.32‰ versus V-PDB (data from Venturi et al., 2019 included) (Table 2). Values from −15.3‰ to −1.8‰ versus V-PDB (mean = −5.61‰ vs. V-PDB) were recorded at Sasso Pisano, while narrower ranges were registered at Sasso-Monterotondo (between −3.9‰ and −0.3‰ vs. V-PDB) even though here only three samples were analyzed (Tables 1 and 2). Soil temperatures in these areas were widely varying, from 10°C to 99°C, with a mean value of 31°C ± 14°C. Soil temperatures higher than 50°C were mainly measured at Monterotondo-N (>20 points) and, more rarely, in the other central areas.

4.1.2. Peripheral Areas

The peripheral areas (Figures 3c and 3d) generally showed higher CO_2 flux values when compared to those registered in the central areas, spanning between 0.5 g m^{-2} day^{-1} (Micciano-SE) up to 72,200 g m^{-2} day^{-1} (Micciano-NW), with mean values ranging from 26 (Micciano-SE) to 2,211 g m^{-2} day^{-1} (Micciano-NW), respectively (Table 2). At Libbiano and Montemiccioli, the mean values are 1,673 and 1,254 g m^{-2} day^{-1}, respectively. The lowest CO_2 soil fluxes pertain to Palazzo al Piano (mean value: 130 g m^{-2} day^{-1}). In the peripheral areas, the carbon isotopic composition of soil interstitial gases was analyzed in Libbiano, Palazzo al Piano, and Montemiccioli localities (Tables 1 and 2). Samples from Libbiano show relatively homogeneous values, ranging between −8.0‰ and −3.9‰ versus V-PDB (mean value: −6.51‰ vs. V-PDB), except for one sample which showed a more negative value (i.e., −16.2‰ vs. V-PDB) (Table 2). Palazzo al Piano interstitial gases have $\delta^{13}C$-CO_2 values ranging between −19.7‰ and −2.5‰ versus V-PDB with a mean value of −11.50‰ versus V-PDB (Table 2). Finally, Montemiccioli shows values similar to those measured at Libbiano, spanning between −12.5‰ and −2.0‰ versus V-PDB (mean value: −6.48‰ vs. V-PDB) (Table 2). Soil temperatures recorded in these peripheral areas range in a narrow interval (i.e., 20°C–40°C; Table S1 in Supporting Information S1) and have a mean value of 28°C ± 6.5°C (i.e., similar to that of the air at the time of the surveys).

Table 2
Estimated Parameters, Partitioned CO_2 Flux Populations and $\delta^{13}C$-CO_2 Values in the Interstitial Gases From the Study Areas

Site	Population	N. measures	Proportion (%)	CO_2 flux (g m^{-2} day^{-1})					N. analyses	$\delta^{13}C$-CO_2 (‰ vs. V-PDB)	
				Min	Max	Mean	St. dev.	Median		Min	Max
				Central areas							
Monterotondo-N	A	14	14	0.2	2.1	1.3	±0.6	1.4	1	−10.2	
	B	64	66	2.9	212	51.5	±62.9	24.1	14	−26.3	+2.2
	C	18	18	268	5,535	1,315.3	±1,496.4	763.1	3	−1.0	+0.05
	Outliers	2	2	21,077	29,837	–	–	–	–	–	
	Total	98	100	0.2	29,837	794.9	±3,719.8	28.2	18	−26.3	+2.2
Monterotondo-S[a]	A	30	34	1.4	7.3	4.0	±1.7	4.2	15	−16.1	−0.53
	B	44	49	7.5	246	49.0	±47.9	32.9	14	−13.7	+3.5
	C	15	17	260	2,144	779.3	±571.4	557.1	6	−10.7	+0.70
	Total	89	100	1.4	2,144	156.9	±364.6	23.1	35	−16.1	+3.5
Sasso-Monterotondo	A	14	19	0.3	2.2	1.3	±0.6	1.3	–	–	
	B	51	68	3.0	137	29.9	±33.6	15.2	–	–	
	C	9	12	207	802	441.4	±204.1	412.5	2	−2.0	−0.28
	Outlier	1	1	3,338		–	–	–	1	−3.9	
	Total	75	100	0.3	3,338	118.0	±407.4	14.4	3	−3.9	−0.28
Sasso Pisano	A	24	59	0.3	28	10.0	±8.8	6.6	1	−8.3	
	B	17	41	44	1,116	470.0	±372.0	281.3	7	−15.3	−1.8
	Total	41	100	0.3	1,116	200.7	±328.7	20.5	8	−15.3	−1.8
Lagoni-Sasso	A	32	43	1.0	18	9.3	±4.5	8.2	–	–	
	B	42	56	22	200	52.3	±40.1	37.2	–	–	
	Outlier	1	1	545		–	–	–	–	–	
	Total	75	100	1.0	545	40.6	±69.6	23.7	–	–	
				Peripheral areas							
Micciano-NW	A	15	23	4.7	41	24.8	±12.2	28.9	–	–	
	B	40	63	49	497	151.3	±106.7	121.6	–	–	
	C	7	11	974	3,368	2,133.5	±1,100.3	1,361.8	–	–	
	Outliers	2	3	47,940	72,200	–	–	–	–	–	
	Total	64	100	4.7	72,200	2,210.9	±10,719.2	91.3	–	–	
Micciano-SE	A	42	86	0.5	26	8.6	±7.0	6.5	–	–	
	B	7	14	46	436	129.9	±140.2	75.7	–	–	
	Total	49	100	0.5	436	25.9	±65.8	10.1	–	–	
Libbiano	A	51	98	3.0	5,845	637.3	±1,215.1	168.8	23	−16.2	−3.9
	Outlier	1	2	54,513		–	–	–	–	–	
	Total	52	100	0.5	54,513	1,673.4	±7,573.3	177.5	23	−16.2	−3.9
Palazzo al Piano	A	69	84	11	62	33.5	±13.3	34.3	4	−19.7	−10.8
	B	13	16	65	3,462	640.1	±1,017.7	185.3	4	−15.0	−2.5
	Total	82	100	0.5	3,462	129.7	±450.9	37.4	8	−19.7	−2.5
Montemiccioli	A	37	33	6.8	22	15.1	±4.1	15.1	1	−12.5	
	B	57	51	23	624	136.2	±148.1	69.7	9	−9.3	−2.0
	C	18	16	921	21,435	7,338.3	±6,844.3	5,038.4	7	−7.6	−6.2
	Total	112	100	6.8	21,435	1,253.7	±3,787.0	50.2	17	−12.5	−2.0

[a]Data from Venturi et al. (2019) and Cabassi et al. (2021).

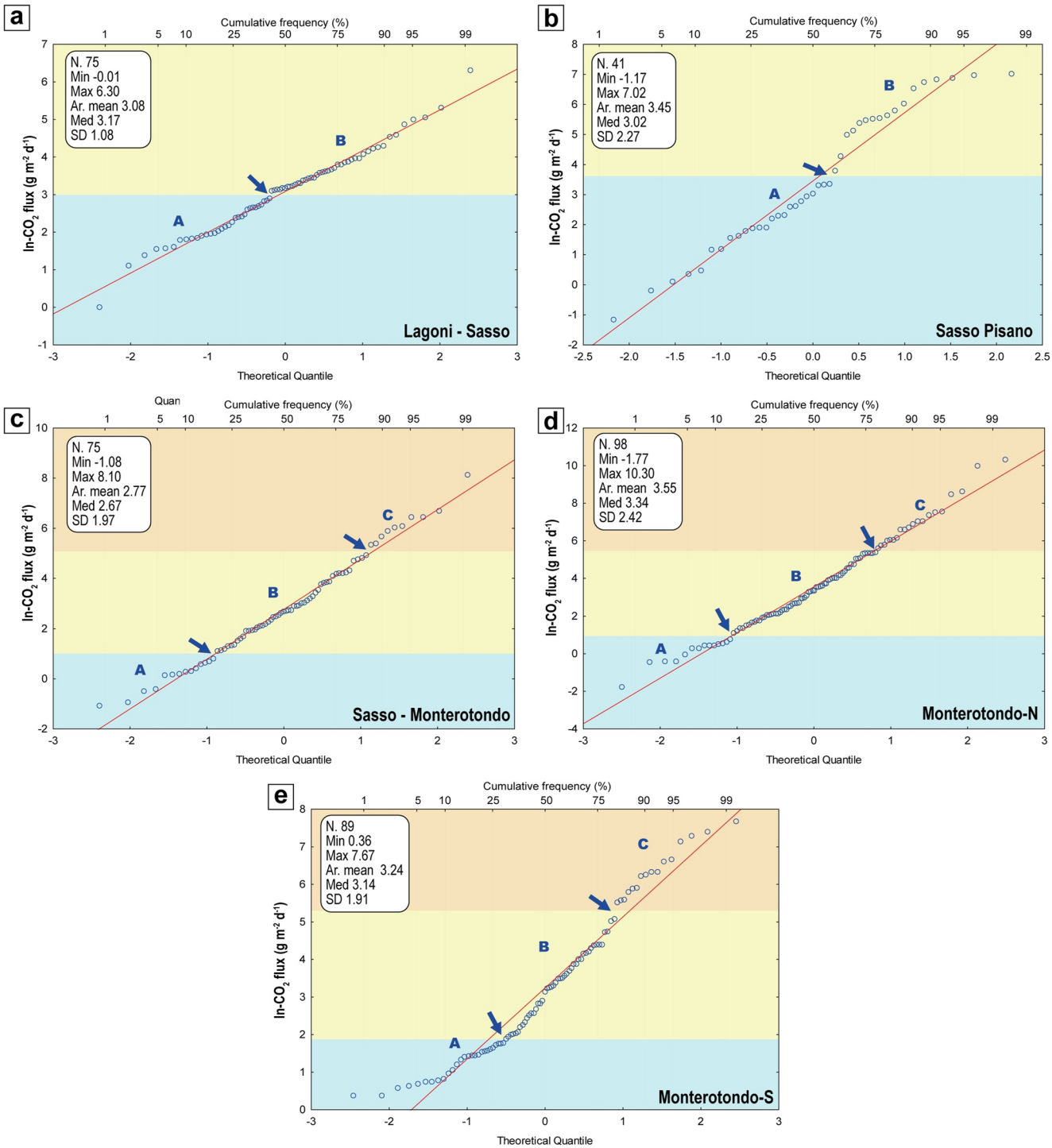

Figure 4. Cumulative frequency plots (ln-values) of soil CO_2 measurements of the central areas from the Larderello geothermal field: (a) Lagoni-Sasso; (b) Sasso Pisano; (c) Sasso-Monterotondo; (d) Monterotondo-N; (e) Monterotondo-S (after Cabassi et al., 2021). The inflection points are reported as blue arrows and the different background colors allow to distinguish the different populations. The red lines represent theoretical (log)normal distributions.

4.2. CO_2 Flux Populations and Distribution Maps

4.2.1. Central Areas

A polymodal distribution of the cumulative frequency plot of the lnϕCO_2 flux data characterizes the central areas of Larderello (Figure 4), suggesting the presence of multiple different (log)normal populations discretized by inflection points.

Moving from North to South, at Lagoni-Sasso and Sasso Pisano (Figures 4a and 4b), one inflection point in each plot is recognized at lnϕCO_2 2.89 and 3.34 g m^{-2} day^{-1} (i.e., ~18 and ~28 g m^{-2} day^{-1}), respectively. Three populations are evidenced in the cumulative frequency diagram of Sasso-Monterotondo (Figure 4c) and Monterotondo-N (Figure 4d), with inflection points at lnϕCO_2 0.80 and 4.92 g m^{-2} day^{-1} (i.e., ~1.3 and ~137 g m^{-2} day^{-1}) and at lnϕCO_2 0.74 and 5.36 g m^{-2} day^{-1} (i.e., ~2.1 and ~212 g m^{-2} day^{-1}), respectively. The latter values are quite in agreement with the CO_2 flux populations recognized by previous studies from Monterotondo (Figure 4e; Cabassi et al., 2021; Taussi et al., 2022). The inflection points identified in Figure 4 discretize low, intermediate, and high flux populations (namely A, B, and C, respectively) (Table 2). The mean values of population A, which represents 14%–59% of the data sets, range between 1.3 and 10 g m^{-2} day^{-1} (Table 2). The intermediate (32%–56% of the measurements) populations (B) have mean values generally ranging from 30 to 85 g m^{-2} day^{-1}, except for Sasso Pisano where population B represents 41% of the data set and has a mean flux value of 470 g m^{-2} day^{-1}. Eventually, the higher flux populations (C) at Sasso-Monterotondo, Monterotondo-N, and Monterotondo-S (12%, 18%, and 17% of the data sets, respectively) have mean values between 441 and 1,315 g m^{-2} day^{-1}. The Monterotondo-N CO_2 fluxes have two outliers (recognized through box-plots; not presented) defined by the highest emitting sites recorded among all the measurements of the central areas (i.e., 21,077 and 29,837 g m^{-2} day^{-1}, respectively). Two other outliers were related at Sasso-Monterotondo (i.e., 3,338 g m^{-2} day^{-1}) and Lagoni-Sasso (i.e., 545 g m^{-2} day^{-1}) (Table 2).

The distribution maps of the CO_2 fluxes in the central areas (Figure 5) show that the highest values refer to different portions of Monterotondo (Figure 5b) and the northern part of Sasso Pisano (Figure 5a). High values (i.e., >100 g m^{-2} day^{-1}) were also found in the northern part and the central-southern portion of Sasso-Monterotondo (Figures 5a and 5b), while only five high-flux spots were measured at Lagoni-Sasso (Figure 5a).

Even though the point data density for carbon isotopic values of the interstitial gas (Figure 6) is not as high as CO_2 flux measurements, it is still remarkable that the results show a strong heterogeneity across the Monterotondo areas, especially in Monterotondo-S (Venturi et al., 2019).

4.2.2. Peripheral Areas

Among the peripheral areas different soil CO_2 flux statistical log-normal populations can be identified in the cumulative frequency plots of Figure 7.

At Micciano-NW two inflection points at lnϕCO_2 3.72 and 5.91 g m^{-2} day^{-1} (i.e., ~41 and ~368 g m^{-2} day^{-1}, respectively) discretize three different populations (Figure 7a). The lower flux population (A), which represent 23% of the data set, has a mean value of 25 g m^{-2} day^{-1}, the intermediate flux population (B), 63% of the data set, shows a mean value of 151 g m^{-2} day^{-1}, while the higher flux population (C) (11%) has a mean value of 2,133 g m^{-2} day^{-1} (Table 2). Two outliers occur at Micciano-NW, emitting 47,940 and 72,200 g m^{-2} day^{-1}, respectively. Differently, in the nearby Micciano-SE, much lower fluxes pertain to two statistical populations defined by one inflection point at lnϕCO_2 3.25 g m^{-2} day^{-1} (i.e., ~26 g m^{-2} day^{-1}), were recorded (Figure 7b). Population A has values ranging between 0.5 and 26 g m^{-2} day^{-1} (mean value: 8.6 g m^{-2} day^{-1}) whilst population B ranges from 46 to 436 g m^{-2} day^{-1} (mean value: 130 g m^{-2} day^{-1}) (Table 2). At Libbiano, a single statistical population (A) was identified (Figure 7c) with values spanning from 3.0 to 5,845 g m^{-2} day^{-1} (mean value: 637 g m^{-2} day^{-1}), with the maximum measured flux (i.e., 54,513 g m^{-2} day^{-1}) recognized as an outlier of the data set. It is worth noting that at Libbiano, the presence of overlapping population cannot be ruled out, but the low number of measurements (n.52) make difficult to statistically discretize robust and significative populations. The Palazzo al Piano cumulative frequency plot (Figure 7d) underlines the presence of two statistical populations (A and B) discretized by an inflection point at lnϕCO_2 4.13 g m^{-2} day^{-1} (i.e., ~62 g m^{-2} day^{-1}). The two recognized populations have mean values of 33 and 640 g m^{-2} day^{-1} and represent 84% and 16% of the data set, respectively. Finally, the Montemiccioli data set shows a polymodal distribution (Figure 7e) characterized by the presence of at least three populations, evidencing two inflection points at lnϕCO_2 3.08 and 6.44 g m^{-2} day^{-1} (i.e., ~22 and ~624 g m^{-2} day^{-1}), respectively. These inflection points discretized a low-flux population (A) represented by 37% of the data set, an intermediate-flux population (B) which constitutes a major part of the measurements (57%), and a high-flux population (C; 18%). The values of population A range between 6.8 and 22 g m^{-2} day^{-1}, with a mean value of 15.1 g m^{-2} day^{-1}. The intermediate values (population B) span between 23 and 624 g m^{-2} day^{-1} (mean = 136 g m^{-2} day^{-1}), while the high-flux population C shows values from 921 g m^{-2} day^{-1} up to 21,435 g m^{-2} day^{-1} and a mean of 7,338 g m^{-2} day^{-1}.

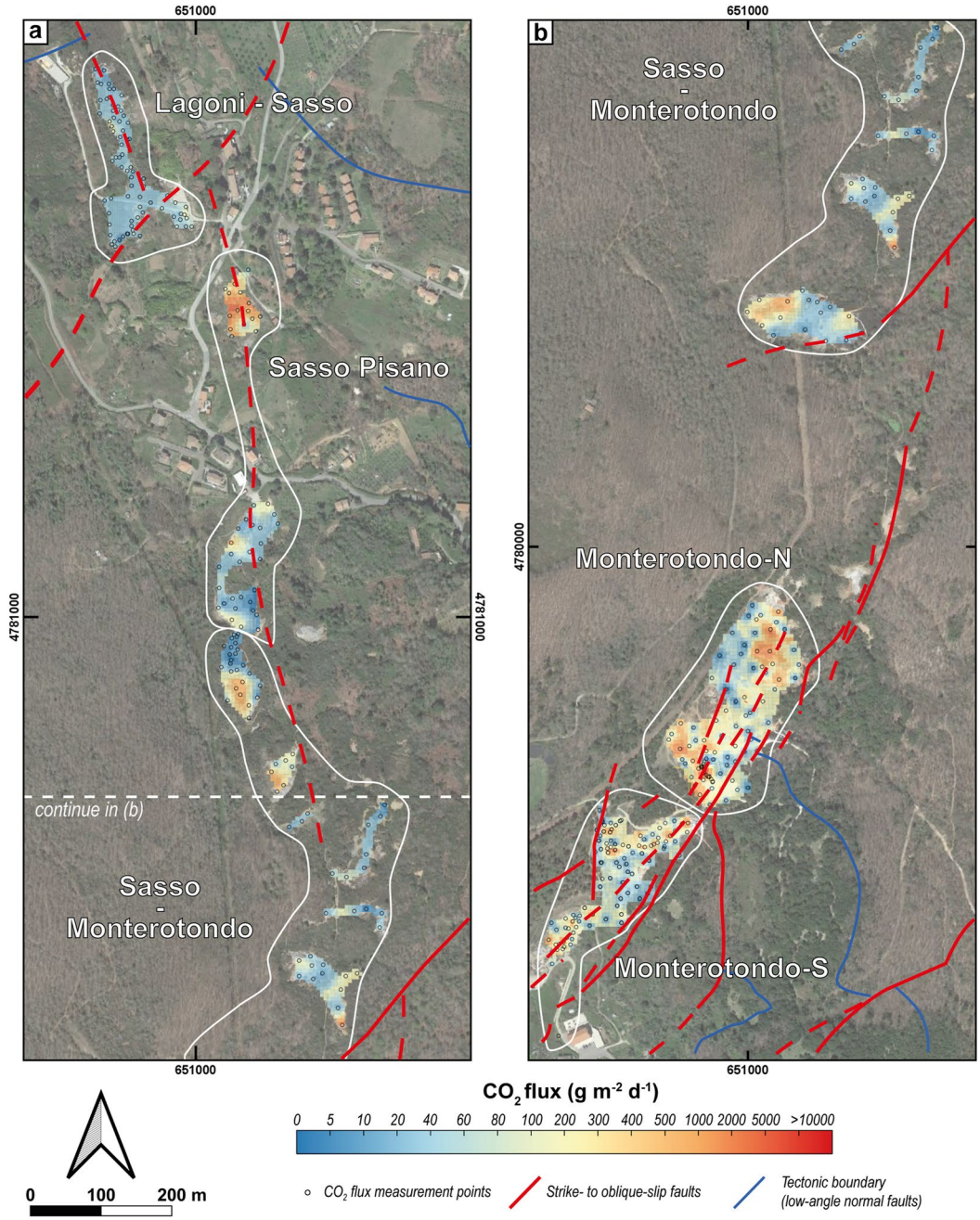

Figure 5. Distribution maps of soil CO_2 flux in the Larderello central areas (from North to South: Lagoni-Sasso, Sasso Pisano, Sasso-Monterotondo, Monterotondo-N, and Monterotondo-S. The data from Monterotondo-S are from Cabassi et al. (2021)). Faults are also reported after Figure 1 and Taussi et al. (2022).

Figure 8 shows the spatial distribution of the CO_2 fluxes measured in the peripheral areas of Larderello. At Micciano (Figure 8a), higher fluxes characterize the NW area with respect to the SE one, where only three points exceed 100 g m^{-2} day^{-1}. However, the different periods of the surveys (i.e., summer vs. winter; Table 1) might have magnified the differences between the two areas (Klusman et al., 2000). At Palazzo al Piano, the higher fluxes (>100 g m^{-2} day^{-1}) are clustered in the central part of the investigated area (Figure 8b). Soil CO_2 fluxes at Libbiano are mostly higher than 100 g m^{-2} day^{-1} (Figure 8c) and are homogeneously distributed in the investigated area. The lower fluxes were measured in the NE portion, where a wooded area is present. Also at Montemiccioli the higher fluxes are quite homogeneously distributed, although in the southern portion they seem to be preferentially distributed along an NS alignment (Figure 8d).

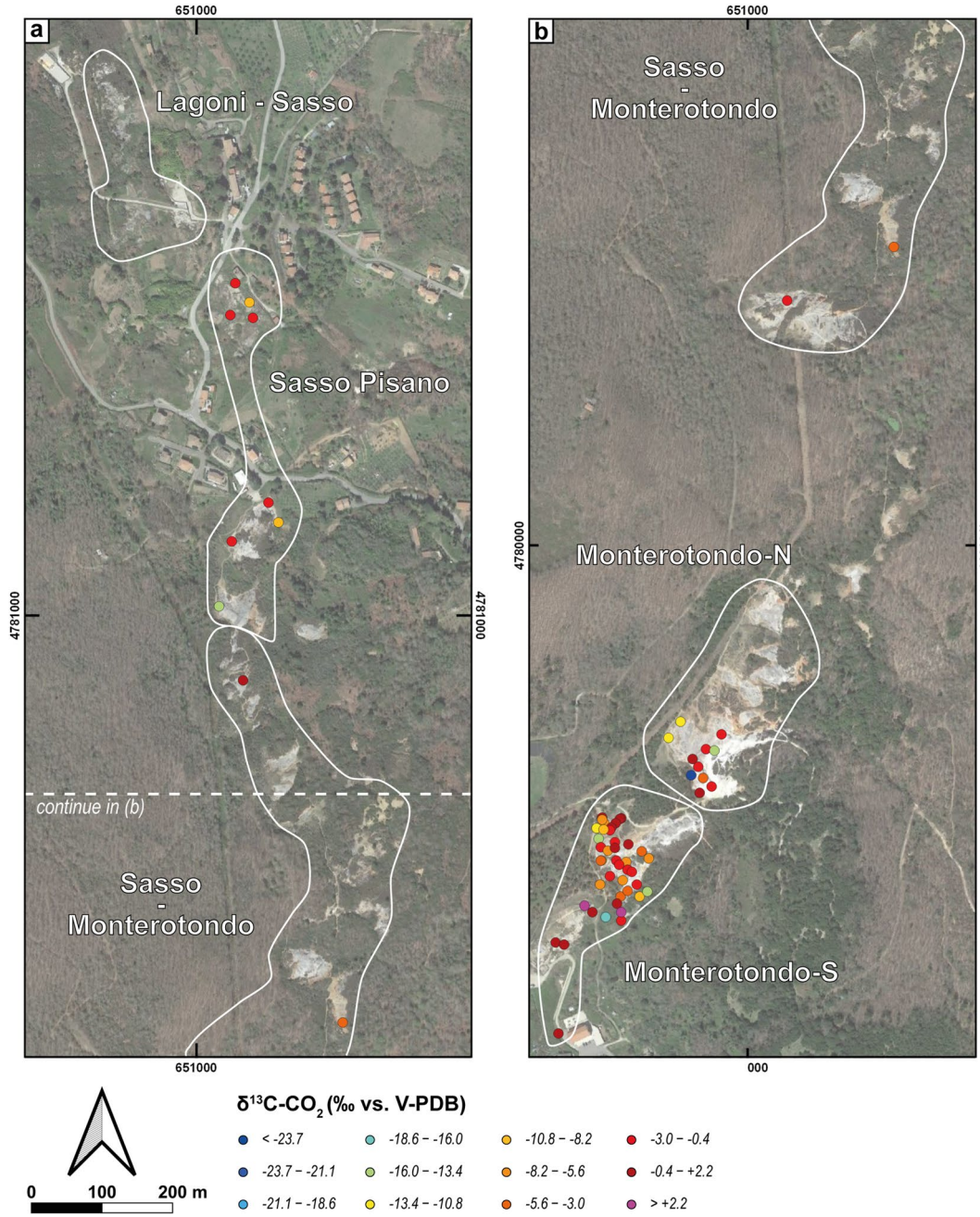

Figure 6. Dot maps of interstitial soil gas $\delta^{13}C\text{-}CO_2$ collected at 20 cm of depth in the Larderello central areas (from North to South: Lagoni-Sasso, Sasso Pisano, Sasso-Monterotondo, Monterotondo-N, and Monterotondo-S (data from Venturi et al., 2019)).

The relatively homogenous isotopic composition of soil gases across the hydrothermalized area of Libbiano (Table 2) is highlighted in Figure 9a, with the most negative value located in the northern part of the zone, measured in an agricultural field. Similar values and a homogeneous distribution throughout the investigated area are also reported for Montemiccioli (Figure 9b). Palazzo al Piano interstitial gases have the less negative $\delta^{13}C\text{-}CO_2$ values occurring in a small area (~18 × 10 m) at the center of the investigated zone, where the highest fluxes were also measured (Figure 8b), while the other more negative values were recorded in correspondence of a maize field (Figure 9c).

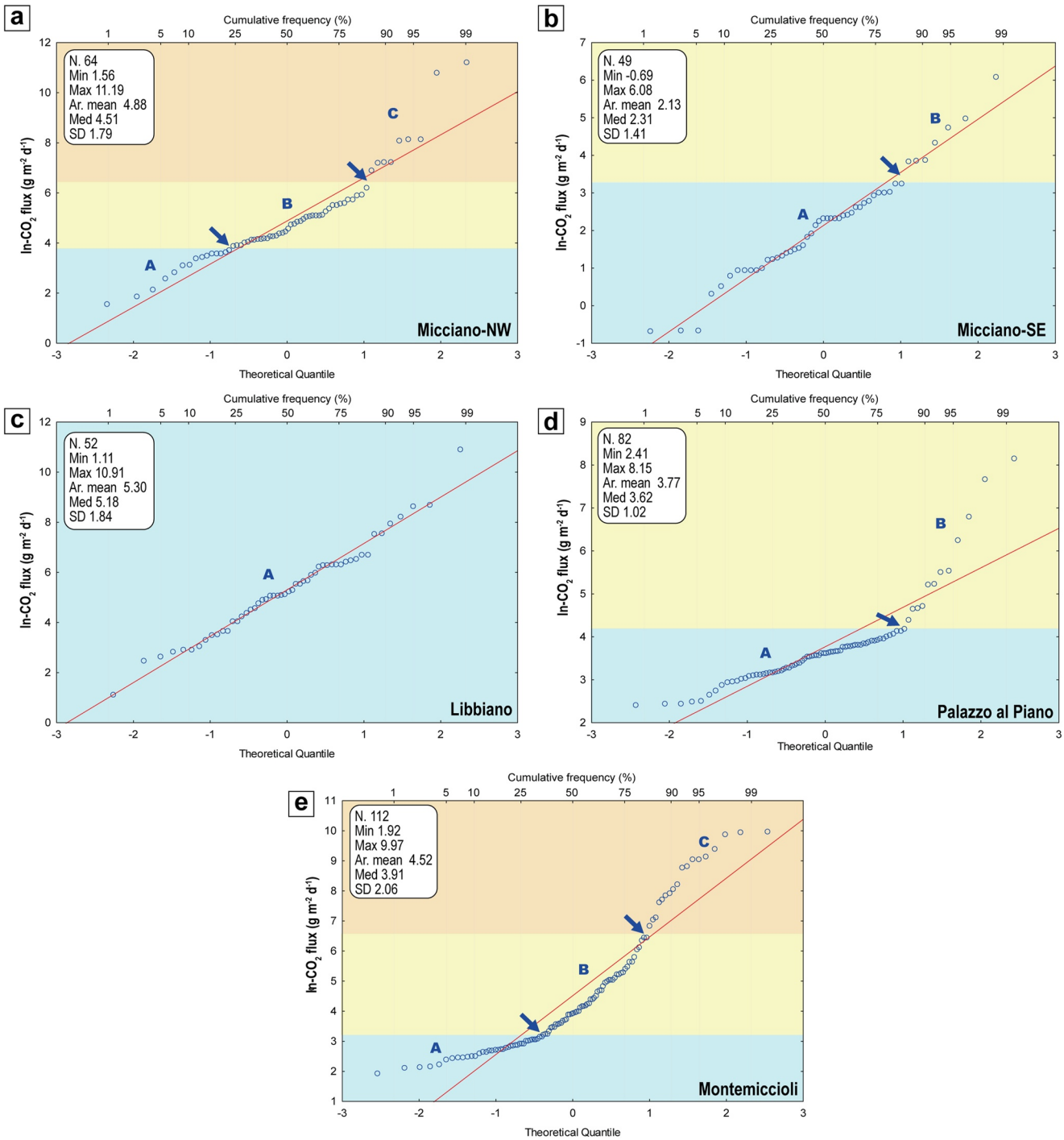

Figure 7. Cumulative frequency plots of ln-values of soil CO_2 measurements of the peripheral areas of the Larderello geothermal field: (a) Micciano-NW; (b) Micciano-SE; (c) Libbiano; (d) Palazzo al Piano; (e) Montemiccioli. The inflection points are reported as blue arrows and the different background colors allow to distinguish the different populations. The red lines represent theoretical (log)normal distributions.

4.3. CO_2 Output Estimations

The estimated total CO_2 outputs from the surveyed areas are reported in Table 3. In the central areas, the values vary between 0.28 and 7.27 t d^{-1}. The lowest values pertain to Lagoni-Sasso, while the highest one belongs to Monterotondo-N. Sasso-Monterotondo and Sasso Pisano release a comparable amount of CO_2, that is, 1.51 and 2.14 t d^{-1}, respectively, whilst 3.15 t d^{-1} of CO_2 were computed for Monterotondo-S (Cabassi et al., 2021).

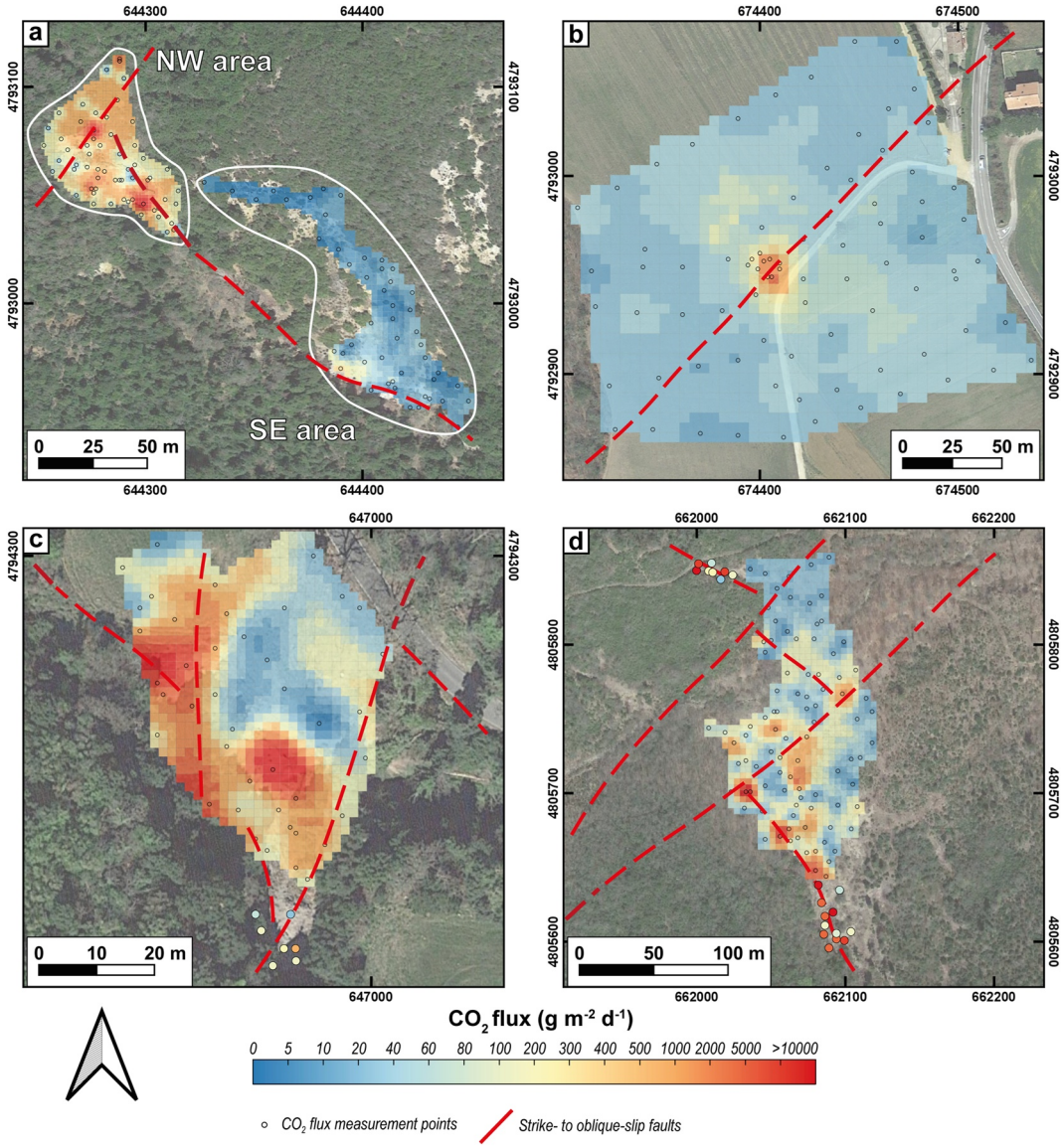

Figure 8. Distribution maps of soil CO_2 flux in the Larderello peripheral areas: (a) Micciano; (b) Palazzo al Piano; (c) Libbiano; (d) Montemiccioli.

In the peripheral areas, the CO_2 output values range from 0.40 t d^{-1} (Micciano-SE) up to 19.77 t d^{-1} (Montemiccioli). Libbiano has a slightly higher output (1.36 t d^{-1}) than that of Micciano-NW (0.90 t d^{-1}), while Palazzo al Piano releases 3.66 tons of CO_2 per day.

5. Discussion

5.1. Soil CO_2 Flux and Interstitial Gas Processes, and Origin of the CO_2

5.1.1. Soil CO_2 Flux Interpretation

The soil CO_2 fluxes span over wide intervals in the investigated areas and multiple populations occur as shown by the cumulative frequency plots (Figures 4 and 7), suggesting the presence of various sources, processes, different soil permeabilities, and/or distinct transport mechanisms of the gases through the soil.

In the central areas, the low flux populations (namely A) show mean values in the order of 1.3–10.0 g m^{-2} day^{-1}, with upper threshold values lower than ~28 g m^{-2} day^{-1} (Figure 4; Table 2). These mean and threshold values agree

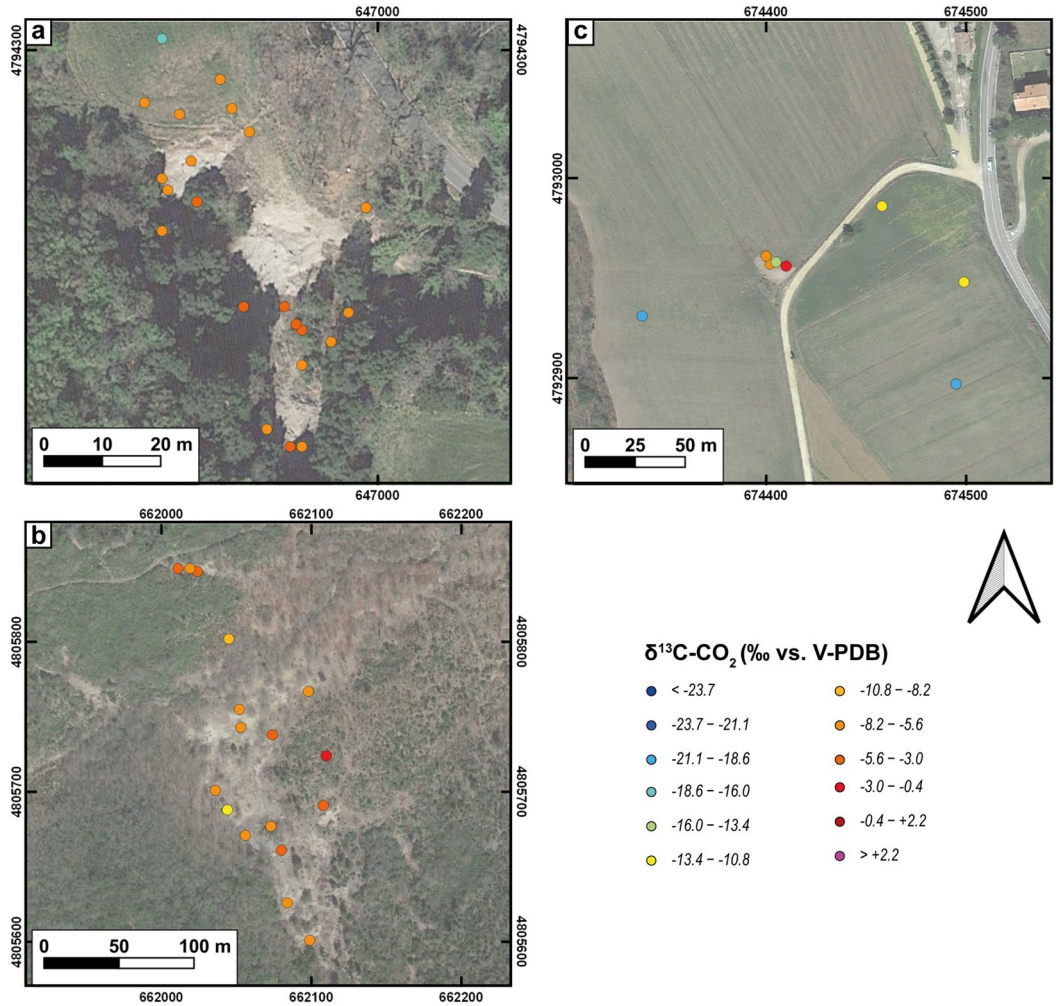

Figure 9. Dot maps of carbon isotopic composition ($\delta^{13}C\text{-}CO_2$) in the interstitial gases collected at 20 cm depth at (a) Libbiano; (b) Montemiccioli; (c) Palazzo al Piano.

with a biogenic source (i.e., plant and microbial respiration and organic decomposition; Cardellini et al., 2003; Chiodini et al., 2008; Raich & Schlesinger, 1992; Viveiros et al., 2010) and are comparable to those registered in other geothermal sites of central Italy, such as Mt. Amiata (Sbrana et al., 2020), Latera (Chiodini et al., 2007) and Torre Alfina (Carapezza et al., 2015). On the contrary, populations C, recognized at Sasso-Monterotondo (Figure 4c), Monterotondo-N (Figure 4d), and Monterotondo-S (Cabassi et al., 2021), represent an endogenous CO_2 source, likely linked to magmatic outgassing and/or decarbonation processes of limestones, carbonates and calc-silicates occurring in these areas (Gherardi et al., 2005). Eventually, given the intermediate mean values computed for populations B, generally comprised between ~30 and ~85 g m^{-2} day^{-1}, they can be related to mixing processes between biogenic and endogenous sources, or different transport mechanisms (i.e., diffusive or advective) as recognized in a specific area of Monterotondo-N (Taussi et al., 2022). An exception is related to population B of Sasso Pisano, where a higher mean value occurs (470.0 g m^{-2} day^{-1}). In this case, it is possible to speculate that the low number of flux measurements (i.e., 44) does not allow a robust statistical interpretation of the cumulative plot (Figure 4b), masking possible inflection points of the curve.

In the peripheral areas, low flux populations (A) at Micciano-NW and -SE, Palazzo al Piano, and Montemiccioli show mean values between 8.6 and 33.5 g m^{-2} day^{-1}, and upper threshold values <62 g m^{-2} day^{-1} (Table 2) argue for a biogenic CO_2 source, in agreement with previous studies in central Italy (Carapezza et al., 2015; Cardellini et al., 2003; Chiodini et al., 2007; Sbrana et al., 2020). At Libbiano, only one statistical population was recognized from the cumulative frequency plot, suggesting a single deep-seated (i.e., endogenous) source, given the mean value of 637.3 g m^{-2} day^{-1}. At Montemiccioli and Micciano-NW, high mean values (i.e., 2,134.5

Table 3
Soil CO_2 Output Estimation From the Study Areas

Site	Population	Output (t d^{-1})	Lower limit (t d^{-1})	Upper limit (t d^{-1})	Total normalized output (t d^{-1} km^2)	Endogenous normalized output (t d^{-1} km^2)[a]
			Central areas			
Monterotondo-N	A	<0.01	–	–		
	B	0.96	0.70	1.48		
	C	6.33	4.45	11.21		
	Outliers	0.002	–	–		
	Total	7.29	5.16	12.70	268.8	268.8
Monterotondo-S[b]	A	0.025	0.025	0.026		
	B	0.44	0.35	0.61		
	C	2.68	2.03	4.16		
	Total	3.15	2.40	4.81	157.5	156.2
Sasso-Monterotondo	A	<0.01	–	–		
	B	0.42	0.32	0.61		
	C	1.09	0.84	1.77		
	Outlier	<0.001	–	–		
	Total	1.51	1.16	2.38	74.6	71.6
Sasso Pisano	A	0.09	0.05	0.19		
	B	2.05	1.46	3.58		
	Total	2.14	1.51	3.77	211.3	202.4
Lagoni-Sasso	A	0.04	0.03	0.05		
	B	0.24	0.21	0.30		
	Outlier	<0.001	–	–		
	Total	0.28	0.24	0.35	32.7	28.1
			Peripheral areas			
Micciano-NW	A	0.02	0.01	0.03		
	B	0.23	0.19	0.29		
	C	0.66	0.44	1.62		
	Outliers	0.004	–	–		
	Total	0.90	0.64	1.94	344.8	337.2
Micciano-SE	A	0.12	0.09	0.19		
	B	0.27	0.16	1.01		
	Total	0.40	0.25	1.20	144.4	101.1
Libbiano	A	1.36	0.83	2.88		
	Outlier	0.002	–	–		
	Total	1.36	0.83	2.88	699.2	699.2
Palazzo al Piano	A	0.86	0.79	0.96		
	B	2.80	1.55	9.01		
	Total	3.66	2.33	9.97	118.4	90.6

Table 3
Continued

Site	Population	Output (t d^{-1})	Lower limit (t d^{-1})	Upper limit (t d^{-1})	Total normalized output (t d^{-1} km^2)	Endogenous normalized output (t d^{-1} km^2)[a]
Montemiccioli	A	0.08	0.07	0.08		
	B	1.01	0.82	1.35		
	C	18.68	12.45	36.84		
	Total	19.77	13.34	38.28	1,320.6	1,315.3

Note. The total and endogenous normalized outputs are also reported.
[a]Intended as the total output to which the background contribution is subtracted. [b]Data from Venturi et al. (2019) and Cabassi et al. (2021).

and 7,338.3 g m^{-2} day^{-1}, respectively; Table 2) are computed for populations C arguing for a purely endogenous source.

At Palazzo al Piano, only two populations were recognized. Population B shows a high mean value of 640.1 g m^{-2} day^{-1}, suggesting an endogenous, or at least mixed source. These values are focused on a small area characterized by the absence of vegetation and small bubbling vents (Tassi et al., 1997; Figure 8b), that is, the only indications of hydrothermalism at Palazzo al Piano.

In the two areas of Micciano and Montemiccioli populations B show intermediate mean values (i.e., 151.3 and 129.9 g m^{-2} day^{-1}, and 136.2 g m^{-2} day^{-1}, respectively; Table 2), suggesting that these fluxes are fed by a mix of biogenic and endogenous sources.

5.1.2. Origin and Processes of the Interstitial Gas

The δ^{13}C-CO_2 values of the interstitial gases show a wide range of variability, spanning from −26.0‰ up to +3.52‰ versus V-PDB. Looking at Figure 10, two non-parametric distributions, marking the differences between the central and peripheral areas, can be highlighted.

Central areas generally show slightly negative up to positive values, mostly grouped between −3‰ and +1‰ versus V-PDB. These values testify general enrichment in ^{13}C, only partially overlapping that reported for both the fumaroles occurring in the central areas (i.e., from −4.2‰ to −2.3‰ vs. V-PDB, Granieri et al., 2023; Leila et al., 2021; Minissale et al., 1997; Tassi et al., 2012; Venturi et al., 2019), and the typical isotopic fingerprint recorded for the Larderello reservoirs geothermal fluids (from −7.1‰ to −1.4‰ vs. V-PDB; e.g., Gherardi et al., 2005). The isotopic range is in good agreement with the typical δ^{13}C-CO_2 values derived by thermo-metamorphic reactions suffered by carbonate rocks (i.e., −5‰ to +5‰ vs. V-PDB; Venturi et al., 2017 and references therein). These processes have indeed been recognized as a significant process of CO_2 production affecting the shallower geothermal reservoir where the major thickness of the Mesozoic carbonate and dolostone rocks has been highlighted (Gherardi et al., 2005; Gianelli et al., 1997). The more negative δ^{13}C-CO_2 values seen in Figure 10 (i.e., <−3‰ vs. V-PDB), are representing either a mantle/magmatic source (i.e., −8‰ to −4‰ vs. V-PDB; Mason et al., 2017) or a mixing between a strongly negative biogenic (i.e., −26‰ vs. V-PDB; Table 2) and an endogenous source, represented by the decarbonation processes.

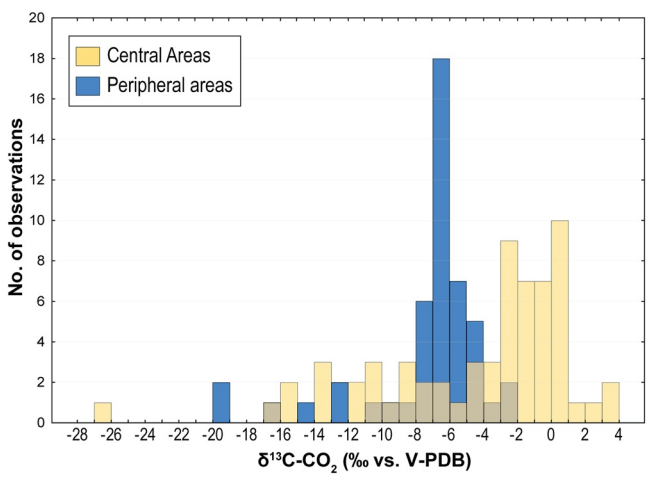

Figure 10. Histograms of the frequency distribution of the interstitial gas δ^{13}C-CO_2 values measured in the central (yellow) and peripheral (blue) areas of the Larderello geothermal field.

Concerning the peripheral areas, the δ^{13}C-CO_2 values frequently fall in the interval −8‰ to −4‰ versus V-PDB, with only a few other points that show more negative values, up to −19.7‰ versus V-PDB (Figure 10). In this case, the isotopic values of the interstitial CO_2 are in good agreement with those measured in the free gases spontaneously emitted from the main vent(s) of each peripheral area. The latter are comprised between −7.3 (Montemiccioli) and −4.7‰ (Palazzo al Piano) versus V-PDB (Minissale et al., 1997; Panichi & Tongiorgi, 1975). These values perfectly fall in the isotopic range of the Larderello reservoirs geothermal fluids (Gherardi et al., 2005), and closely resemble the typical mantle/magmatic signature (Mason et al., 2017). Values

lower than −8‰ versus V-PDB were recorded at Libbiano (n.1: −16.2‰ vs. V-PDB), Palazzo al Piano (n.5: between-19.7‰ and −10.8‰ vs. V-PDB), and Montemiccioli (n.1: −12.5‰ vs. V-PDB). The negative values occurring in the former two areas are located in a maize agricultural field where no evidence of hydrothermalism occurs (Figures 9a and 9c), suggesting a possible biogenic origin related to C4 plants (i.e., −16‰ to −9‰ vs. V-PDB; e.g., Sharp, 2017). On the contrary, at Montemiccioli, no C4 plants are present, likely indicating that the −12.5‰ versus V-PDB value is due to a mixing process between a strongly negative biogenic source (e.g., C3 plants: −33‰ to −23‰ vs. V-PDB; e.g., Sharp, 2017) and a slightly negative endogenous source.

5.1.3. Reconciling Soil CO_2 Flux and Interstitial Gas Interpretations

To reconcile the information derived by the $\delta^{13}C$-CO_2 values of the interstitial gas and the soil CO_2 flux populations, both variables are plotted in Figure 11. In this figure, the $\delta^{13}C$ of the CO_2 emitted from the main vent(s) collected in the studied areas (Libbiano: Panichi & Tongiorgi, 1975; Montemiccioli, Palazzo al Piano: Minissale et al., 1997; Sasso Pisano: Minissale et al., 1997; Tassi et al., 2012; Monterotondo: Venturi et al., 2019; Leila et al., 2021; Granieri et al., 2023) is reported as straight vertical bars. The $\delta^{13}C$-CO_2 ranges of the Larderello geothermal fluids (Gherardi et al., 2005), and other relevant geochemical features (Gianelli et al., 1997; Mason et al., 2017; Panichi et al., 1974; Sharp, 2017) are also plotted for comparison. Despite the high measured CO_2 fluxes (i.e., >200 g m^{-2} day^{-1}), some differences with the expected carbon isotopic fingerprint are detectable (Table 2).

In the central areas, only a few high CO_2 flux measurements show a $\delta^{13}C$-CO_2 value close to that of the fumaroles. Most of them are characterized by more positive values, also with respect to the isotopic fingerprint of the fluids hosted in the Larderello geothermal reservoirs (Gherardi et al., 2005). These differences between the $\delta^{13}C$ values of the CO_2 of the interstitial gases and that of the free gases can be derived by secondary fractionation processes, as observed in many geothermal/volcanic environments such as at Solfatara (Italy; Federico et al., 2010), Vulcano (Italy; Camarda et al., 2007), Planchón-Peteroa Volcanic Complex (Chile; Lamberti et al., 2021), and Ohaaki (New Zealand; Rissmann et al., 2012) among the others.

In the Larderello central areas, the secondary isotopic modifications seem to be mainly related to either microbial consumption at shallow depths (Cabassi et al., 2021; Venturi et al., 2019), resulting in a ^{13}C-rich residual CO_2 in the interstitial soil gases (e.g., Tassi et al., 2015; Venturi et al., 2019), or methanogenic processes. These latter take place in hydrothermal reducing environments that favor the reduction of CO_2 to CH_4 to produce a kinetic isotope effect for carbon, leading to the enrichment of ^{13}C in the residual CO_2 (Whiticar, 1999). Furthermore, transport-driven and boiling fractionation processes linked to the different structural features of the rock mass have also been recognized in these areas (Taussi et al., 2022).

Consequently, the partial inconsistency between the soil CO_2 flux values and the $\delta^{13}C$-CO_2 values of the interstitial gases makes it difficult to unequivocally ascribe the origin of each CO_2 flux population, suggesting that a detailed sampling through soil depth-profiles should be carried out to improve the understanding of these secondary processes and better constraint the origin of the CO_2 (Camarda et al., 2007).

Fractionation processes of the carbon isotopes at shallow depths seem to be less marked in the peripheral areas. At Libbiano, the sole deep-originated (endogenous) statistical population recognized from the cumulative frequency plot (Figure 7c) is associated with a quite homogeneous isotopic composition of the interstitial CO_2, mainly varying between −8.0‰ and −3.9‰ versus V-PDB, in good agreement with the isotopic composition of the CO_2 emitted from the main vent(s) (i.e., −5.9‰ vs. V-PDB; Panichi & Tongiorgi, 1975).

At Palazzo al Piano, the more negative carbon isotopes linked to C4 plants (i.e., <−10.8‰ vs. V-PDB) (Figures 7 and 9; Table 2) are mostly in association with fluxes related to the population A. At the same site, population B fluxes are linked to interstitial gases where the $\delta^{13}C$-CO_2 values roughly approach that of the CO_2 emitted from the main vent(s) (i.e., −4.7‰ vs. V-PDB; Minissale et al., 1997), spanning between −6.0‰ and −2.5‰ versus V-PDB. Nevertheless, one high-flux point (i.e., 515 g m^{-2} day^{-1}) showed a much more negative value (i.e., −15.0‰ vs. V-PDB), which could result by mixing between the endogenous source and a marked biological negative CO_2 source, or alternatively, by fractionation processes likely enhanced by the low permeability (Camarda et al., 2006, 2007) of the clayey soil occurring in that point (Figure S25 in Supporting Information S1).

At Montemiccioli, despite the presence of a mean (15.1 g m^{-2} day^{-1}) and an upper threshold (21.8 g m^{-2} day^{-1}) value of the CO_2 fluxes of the population A, that argues for a biogenic source, the only isotopic analysis related to this population (i.e., −12.5‰ vs. V-PDB; Table 2), seems to indicate at least a mixed origin, given the absence

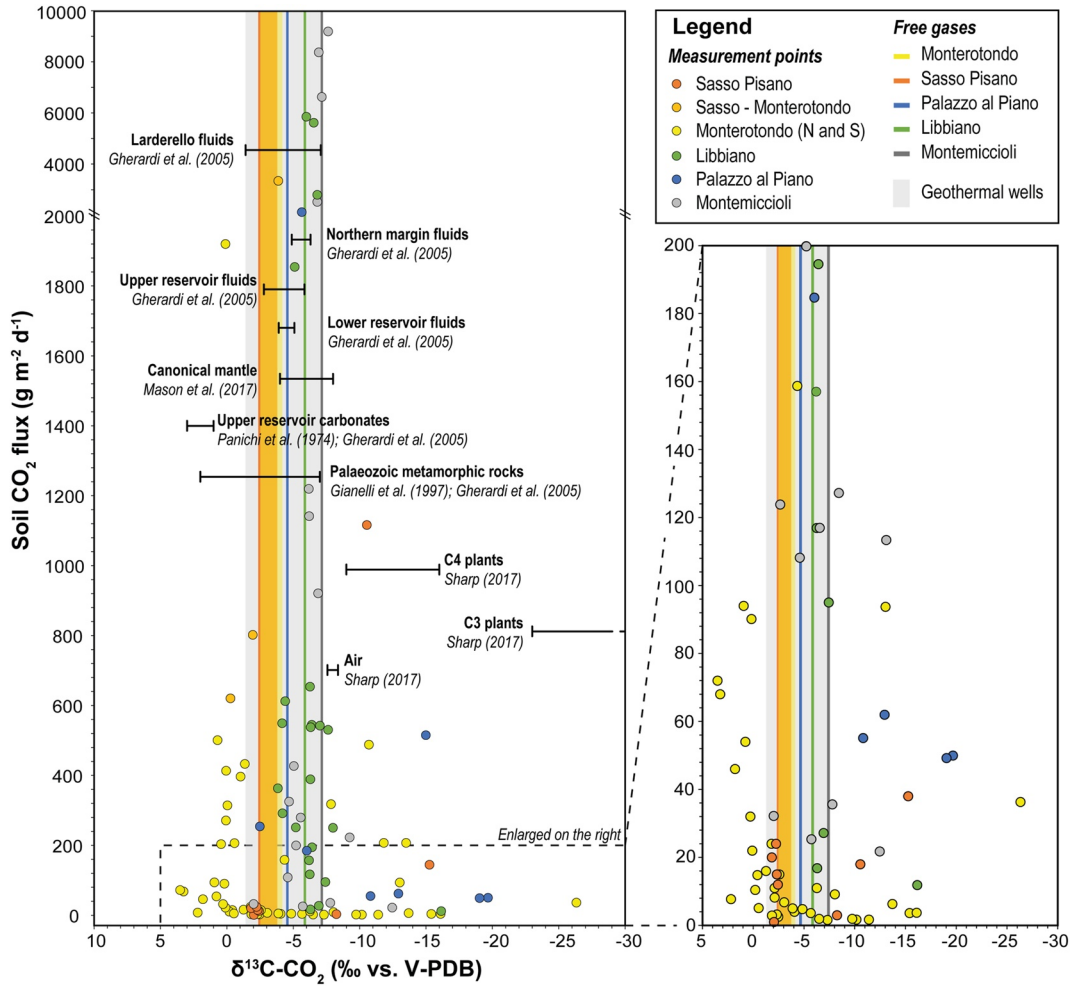

Figure 11. Plot illustrating soil CO_2 fluxes versus corresponding carbon isotopic composition of the interstitial CO_2; previously published carbon isotopic data from Larderello geothermal fluids (Gherardi et al., 2005), CO_2 emitted from the main vent(s) occurring in the investigated areas (Libbiano: Panichi & Tongiorgi, 1975; Montemiccioli, Palazzo al Piano: Minissale et al., 1997; Sasso Pisano: Tassi et al., 2012; Monterotondo: Venturi et al., 2019; Leila et al., 2021) and represented as vertical straight bars, canonical mantle (Mason et al., 2017), Palaeozoic metamorphic rocks (Gherardi et al., 2005; Gianelli et al., 1997), upper reservoir carbonates (Gherardi et al., 2005; Panichi et al., 1974), C3 and C4 plants and air (Sharp, 2017) are reported for comparison.

of C4 plants in this zone. In this area, populations B and C show overlapping isotopic values ranging (a) between −7.8‰ and −2.0‰ versus V-PDB (except for one value of −9.2‰ vs. V-PDB), and (b) from −7.6 to −6.2‰ versus V-PDB, respectively, with the latter, closely resembling that of the CO_2 emitted from the main vent(s) (i.e., −7.3‰ vs. V-PDB; Minissale et al., 1997; Figure 11). A possible explanation for this similarity in the $\delta^{13}C$-CO_2 values of the two different populations might be found in the transport mechanism of CO_2 that can affect the isotopic fractionation. Population B can be related to a mix of diffusive and advective processes to produce enrichment in the heavier carbon isotopes of CO_2 with respect to the that of the gas vents (Federico et al., 2010; Rissmann et al., 2012), likely widening the C-isotopic range of values. Population C is to be linked to purely advective transport, producing almost negligible fractionation and preserving the CO_2 isotopic signature of the reservoir feeding the main vent(s) (Camarda et al., 2007; Capasso et al., 2001; Rissmann et al., 2012; Taussi et al., 2022).

In the two areas of Micciano, no isotopic analyses of interstitial soil CO_2 are available. However, populations B of both areas show mean values (i.e., 151.3 and 129.9 g m^{-2} day^{-1}, respectively) similar to that of Montemiccioli (i.e., 136.2 g m^{-2} day^{-1}; Table 2), suggesting that these fluxes are fed by a mix of shallow (i.e., biogenic) and deep (i.e., endogenous) sources transported by a mix of diffusive-advective processes. In the same way, the high

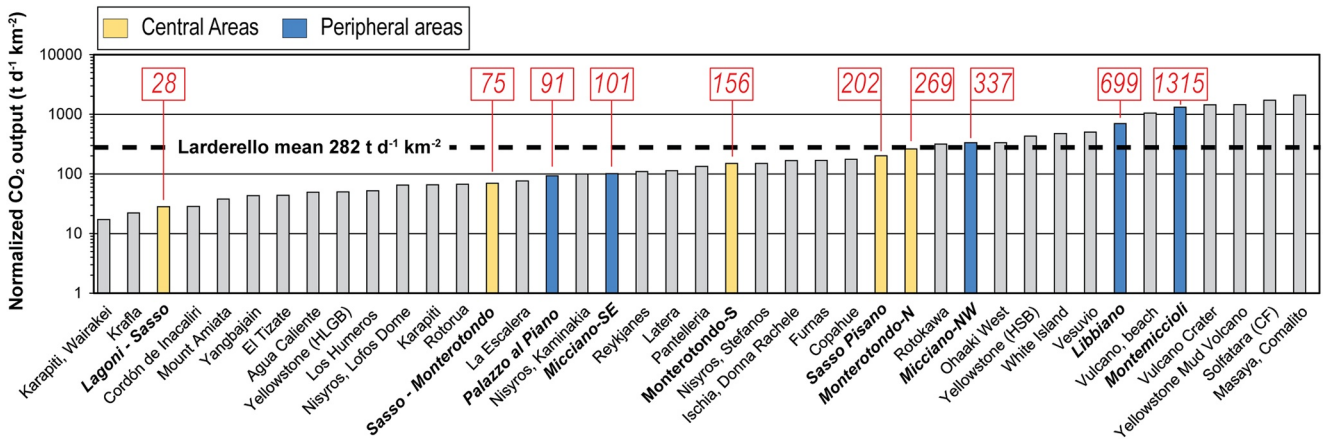

Figure 12. Plot of the mean normalized endogenous CO_2 diffuse emissions for the Larderello geothermal system (including both central and peripheral areas) and the mean value for all the investigated areas, compared with selected worldwide geothermal systems and volcanic areas (after Taussi et al., 2021).

mean value (i.e., 2,133.5 g m^{-2} day^{-1}; Table 2) of population C of the Micciano-NW area argues for a purely deep source, transferred to the surface by an advective mechanism controlled by a pressure gradient.

5.2. CO_2 Budget

A total amount of at least 40.5 tons of CO_2 is emitted every day (~14,260 tons per year) from the investigated hydrothermalized degassing soils of the Larderello geothermal field and neighboring areas, most of them released from Montemiccioli (i.e., ~20 t d^{-1}) and the other peripheral areas (i.e., ~5 t d^{-1}) (Table 3). A total amount of 1.25 t d^{-1}, corresponding to ~450 t y^{-1}, is related to the local background, characterized by a biogenic source and secondary, shallow-depths fractionation processes. The endogenous output of Larderello is one order of magnitude lower than the global mean value (~180,000 tons CO_2 y^{-1}), estimated by Fischer et al. (2019), for the volcanic-hydrothermal CO_2 emitted by diffuse emission from volcanic/geothermal soils worldwide. Nevertheless, the computed CO_2 output is to be regarded as a minimal estimate of the total natural soil emissions from the Larderello geothermal field, considering that other areas of diffuse degassing are present (e.g., Lagoni Rossi, San Pompeo, Lago Boracifero, Monteguidi, Tignano, Castelletto, among the others; Figure 1). These sites, however, were not investigated due to access difficulties or small degassing areas, and, to the best of our knowledge, no CO_2 flux measurements are available. Moreover, the surveyed areas have different extensions (Table 1), which makes unreliable a direct comparison in terms of CO_2 output. Thus, a consistent way to compare the total emission values of different-size surveyed areas among each other—and with other geothermal systems worldwide—is to consider the normalized total CO_2 flux from soil (i.e., the total output divided by the area of the survey). In this case, marked differences between the central and the peripheral areas can be highlighted (Figure 12).

The cold-degassing areas located at the periphery of the geothermal system show high-to-very-high normalized CO_2 outputs. Micciano-SE and Palazzo al Piano emit ~101 and ~91 t d^{-1} km^{-2} of deeply derived CO_2, while Micciano-NW, Libbiano, and Montemiccioli discharge ~333, ~699, and ~1,315 t d^{-1} km^{-2} (Table 3) of deep CO_2, respectively, the latter representing the farthest emission area from the center of the geothermal field (Figures 1 and 3). These values are much higher with respect to some important Italian (e.g., Latera, Pantelleria, Mt. Amiata) and global geothermal fields in the world, such as Los Humeros (Mexico), Rotorua (New Zealand), or Reykjanes (Iceland), and comparable to some of the most active volcanic systems on Earth, as Vulcano (Italy) and Yellowstone (USA), among the others (Figure 12).

In the central areas, two peaks of ~269 (Monterotondo-N) and ~202 (Sasso Pisano) t d^{-1} km^{-2} of endogenous CO_2 are computed (Figure 11; Table 3). Moving away from these areas, CO_2 output values of ~28 (Lagoni-Sasso) and ~75 t d^{-1} km^{-2} (Sasso-Monterotondo), being one order of magnitude lower than those of Monterotondo-N and Sasso Pisano, are calculated. The Monterotondo-S shows an intermediate value of ~156 t d^{-1} km^{-2} (Cabassi et al., 2021).

A recent paper, published by Granieri et al. (2023), highlighted some differences in the calculated CO_2 output in the Monterotondo area (encompassing both Monterotondo-S and -N; i.e., 195 t d^{-1} km^{-2}) than that computed

by Cabassi et al. (2021) for Monterotondo-S. This was justified by the different approaches used for defining the total CO_2 emitted for this area (i.e., sequential Gaussian simulation vs. GSA). Nevertheless, when comparing the normalized CO_2 outputs obtained by Granieri et al. (2023), Cabassi et al. (2021), and this work no significant differences can be found since the amount of CO_2 from these areas are perfectly comparable when both Monterotondo areas (-S and -N) are considered (i.e., ~210 t d^{-1} km^{-2}), hence, suggesting that the calculation procedures used in this and in the previous papers are correct.

As previously stressed, near the core of the Larderello geothermal field the normalized CO_2 outputs are generally lower than those computed for the peripheral ones. These marked differences might be related to the influence of the geothermal production activities, as suggested by various authors (Bertani & Thain, 2002; Duchi et al., 1992; Lenzi et al., 2021) which reported a visible decrease in the natural emissions of the Larderello geothermal field during the years. This is similar to what was observed at Mt. Amiata (Italy; Frondini et al., 2009), another Tuscan geothermal system located about 70 km to the Larderello SE. Pre-production emissions at geothermal industrial sites are often lacking since development began when environmental effects were not monitored (Manzella et al., 2018). Nevertheless, an approximation of the pre-production emissions of CO_2 at the Larderello geothermal area was computed by Lenzi et al. (2021) based on the historical production of boric acid. These authors calculated an average flux rate of Non-Condensable Gases (NCG, composed by 97.7% CO_2) in the geothermal fluid, from the entire historical production area, ranging between ~0.48 and ~15.4 t h^{-1} in the period 1818–1857, which roughly corresponds to ~11 to ~360 t d^{-1} of CO_2. In addition, an estimation for the Sasso Pisano and Monterotondo areas was carried out with data from 1867. This corresponded to a total NCG flow rate of ~3.6 t h^{-1}, that is, a value of ~84 t d^{-1} of CO_2, which is about 5.5 times the output calculated for the central areas in this work (Table 3).

The gradual decline in gas emissions from geothermal sites might be related to, for example, the local influx of short-time circulation path and gas-free recharge water triggered by exploitation that lower the NCG gas content (Romagnoli et al., 2010), and/or to reinjection of the geothermal fluids. For example, Jentsch et al. (2021) recently found a negative correlation between reinjection rates and CO_2 fluxes at the Los Humeros geothermal field (Mexico). Reinjection of the CO_2-depleted geothermal fluid back into the reservoir, which started in the 1970s at Larderello (Minissale, 1991), would likely reduce the CO_2 concentration of the reservoir, leading the reinjected fluid to absorb deep free carbon dioxide gases from the reservoir in the liquid phase (Fridriksson et al., 2017; Kaya & Zarrouk, 2017). Nevertheless, this is somehow in contrast with what assessed by Gherardi et al. (2005), which found no marked difference between the pre- and post-reinjection fluids concentrations and C-isotopic content, suggesting that this process should be further studied.

However, changes in terms of the surface release of CO_2 may vary from place to place (Fridriksson et al., 2017). In fact, at the Wairakei, Ohaaki (New Zealand; Allis, 1981; Rissman et al., 2012) and Reykjanes (Iceland; Fridriksson et al., 2006; Óladóttir & Fridriksson, 2015) geothermal systems, the emitted CO_2 increased along with the geothermal production activities. In these cases, as the pressure declines in the high-temperature productive reservoirs the boiling at depth increases, implying an increased surface activity (Fridriksson et al., 2017).

5.3. Structural Control on CO_2 Degassing

The relation between faults and CO_2 distribution is defined in several contexts (e.g., Gianmanco et al., 1997; Jung et al., 2014; Li Vigni et al., 2022; Miao et al., 2020; Taussi et al., 2021) demonstrating that permeability is partitioned along the fault trace (Jolie et al., 2016), determining different amount and origin of the CO_2 degassing at surface. This is also our case study. Carbon dioxide emissions and geothermal manifestations are indeed concentrated in the SW portion of the Larderello geothermal system (Figure 13a), where the signature of stable isotopes of the CO_2 (Figure 13b) and the $^3He/^4He$ isotopic ratios (Figure 13c) suggest a deep circuit. At the same time, emissions outside these areas reveal a still deep-sourced CO_2, but with a major contribution of shallower processes. It is also worth noting that all the CO_2 emissions and geothermal manifestations are located on fault traces being part of the transfer zone along which the Larderello geothermal system is developing (Figures 1 and 13a). Such evidence sheds light on the fact that the transfer zone, for its crustal relevance, crosses a heterogeneous crust and hosts compartmentalized geothermal circuits. Permeability is also variable along the structure, prevailing in localized sectors where NE-striking faults form highly damaged rock volumes crossing a relevant crustal sector. The deep-seated fluids emerging in the central areas of the Larderello geothermal field from the very low permeable deposits filling the Lago basin suggest converging factors, that is, (a) the permeability of faults is tectonically maintained as indicated by the local earthquakes (Albarello et al., 2005; Bagagli et al., 2020; Liotta & Brogi, 2020); (b) the fault segments have regional relevance (Liotta & Brogi, 2020); (c) the active magmatism (Farina et al., 2018;

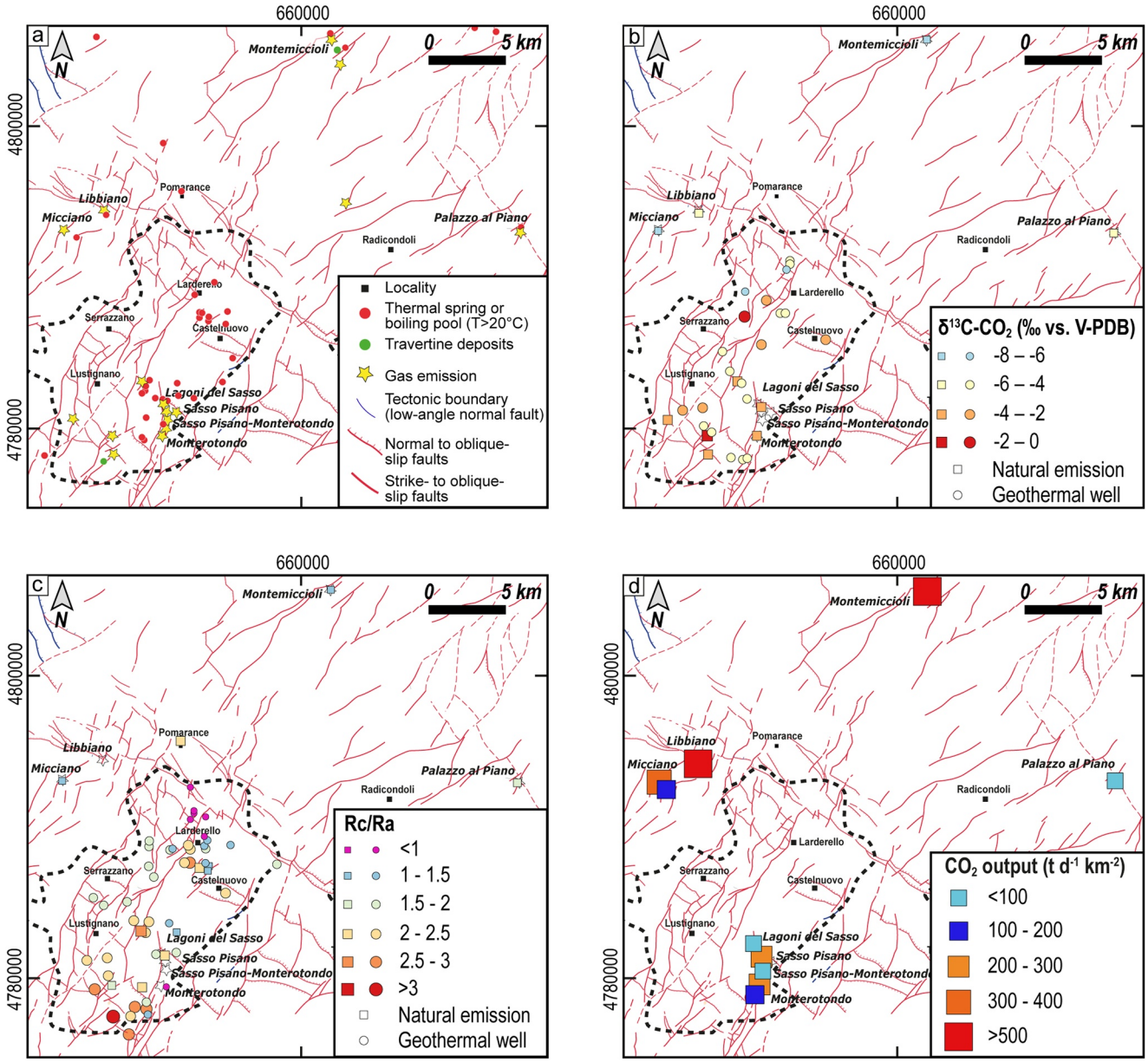

Figure 13. (a) Map showing the main geological structures and geothermal manifestations occurring at the Larderello geothermal field; (b) dot-map of the $\delta^{13}C$ values of the CO_2 in natural emissions (data from Granieri et al., 2023; Hooker et al., 1985; Leila et al., 2021; Minissale et al., 1997; Panichi & Tongiorgi, 1975; Tassi et al., 2012; Venturi et al., 2019) and geothermal wells (Gherardi et al., 2005; Magro et al., 2003); (c) dot-map of the Rc/Ra values measured in natural emissions (data from Hooker et al., 1985; Minissale et al., 1997; Magro et al., 2003) and geothermal wells (Gherardi et al., 2005; Hooker et al., 1985; Magro et al., 2003); (d) distribution of degassing rates computed in this work for central and peripheral areas. The black dashed lines circumscribe the location of most of the geothermal wells drilled in the area (after www.geothopica.igg.cnr.it).

Rochira et al., 2018) favors the uprising of deep-originated fluids (Gola et al., 2017). Outside the central areas, the fault segments belonging to the transfer zone still have considerable importance in terms of permeability, as evidenced by the fact that CO_2 emissions occur in areas dominated by poorly permeable rocks (i.e., clay and silt). Such a permeability within the deeper crustal levels suggests the propagation of the transfer zone even below the upper crust, possibly inheriting the geometrical setting of pre-existing structures (Liotta, 1991).

In the central areas and surroundings, the highest heat flux values of the Larderello geothermal area have been measured, reaching up to ~1,000 mW m^{-2} (Della Vedova et al., 2001), with soil temperatures reaching up to ~98°C in correspondence with geothermal emergencies (Cabassi et al., 2021; Taussi et al., 2022). These conditions mainly occur along an NNE-striking fault zone, at least 5 km long, that runs from Monterotondo Marittimo to Sasso Pisano

(Liotta & Brogi, 2020). The computed differences in the emission rates among Monterotondo (N and S), Sasso Pisano, and Lagoni-Sasso areas might thus be found in the different permeability values enhanced by faults and fractures characterizing the rock volume (Taussi et al., 2022). The areas of Monterotondo are likely hosting the largest number of geothermal manifestations (e.g., fumaroles, steam vents, acidic and steam-heated boiling pools, and mud pools; Minissale, 1991; Duchi et al., 1992) when compared to other Larderello degassing sites (Figure 13a) and display highly pervasive faults and fractures that reach the surface and modulate the fluid discharges (Taussi et al., 2022).

Usually, soil CO_2 flux from the peripheral areas of a volcanic or geothermal system is lower compared to that measured at the summit or core areas (e.g., D'Alessandro et al., 1997; S. Inguaggiato et al., 2013; Jolie et al., 2019; Varley & Armienta, 2001). Nevertheless, cold degassing sites located outside the productive area, are significant emitters of diffuse CO_2 from the Larderello geothermal system (Figure 13d), with degassing rates of CO_2 higher than those of the thermally active central areas (Figures 12 and 13d; Table 3). These marked differences can be related to a high deeply sourced CO_2 flux from the geothermal reservoir that interacts with shallow meteoric groundwater and is then degassed at shallow levels, with the consequent removal of the steam component. Similar behavior has been observed at Yellowstone (Rahilly & Fischer, 2021), where cold degassing sites located outside the caldera rim showed degassing rates comparable to those of the acid-sulfate thermal soils located inside. To achieve these high degassing rates, the shallow aquifer(s) must be cool enough to avoid steam formation which would produce an elevated superficial heat flux (Rahilly & Fischer, 2021 and references therein), but it should also be unable to buffer and mask the CO_2 released by the geothermal system (C. Inguaggiato et al., 2017; Minissale, 2018; Taussi et al., 2019). However, the northern part of the Larderello geothermal field and its hydrogeological setting is still unclear (Minissale, 1991), and it is thought that the shallow aquifers do not, or slightly, interact with the shallow geothermal reservoir (Romagnoli et al., 2010). Nonetheless, the northern margin of the geothermal field is characterized by widespread condensation in the geothermal wells that could be attributed to the very low permeability of the reservoir in this area, leading to large conductive heat losses of the steam in the wells (Minissale, 1991), likely deriving from deep-rooted faults connected with the lower reservoir.

The connection of peripheral cold degassing sites with the geothermal system seems to be supported by the $\delta^{13}C\text{-}CO_2$ values of the free gas discharged from the main vent(s) (Figure 13b), which fall within the range of $-7.1‰$ to $-1.4‰$ versus V-PDB measured in the Larderello geothermal wells (Gherardi et al., 2005). Indeed, the C-isotopic values vary between -4.7 (Palazzo al Piano: Panichi & Tongiorgi, 1975) and $-7.3‰$ V-PDB (Montemiccioli: Minissale et al., 1997), suggesting that a significant proportion of the CO_2 reaching these areas is fed by an endogenous source. Moreover, the isotopic helium ratios of the peripheral area of Micciano, Montemiccioli, and Palazzo al Piano vary between 1.21 and 1.81 (mean Rc/Ra: 1.43; Minissale, 2004; Minissale et al., 1997; Figure 13c), which are slightly lower than the Rc/Ra range (1.63–3.2 Ra) of the gases measured in the system core (i.e., Lago, Le Prata, Sasso Pisano, S. Pompeo; mean Rc/Ra: 2.47; Hooker et al., 1985; Minissale et al., 1997; Magro et al., 2003; Figure 13c).

The isotopic composition ($\delta^{13}C\text{-}CO_2$ and Rc/Ra) of the gases discharged in the central and peripheral areas (data from Minissale, 2004; see Table S1 in Supporting Information S1) is plotted against each other in Figure 14a. Four possible sources are reported, representing (a) the canonical mantle (Rc/Ra = 8 ± 1 and $\delta^{13}C\text{-}CO_2 = -6.5‰ \pm 2.5‰$ vs. V-PDB; Sano & Marty, 1995), (b) the European Subcontinental Mantle (Rc/Ra = 6.3 ± 0.4 and $\delta^{13}C\text{-}CO_2 = -3.25‰ \pm 1.75‰$ vs. V-PDB; Dunai & Baur, 1985; Gautheron et al., 2005; Rizzo et al., 2018), (c) an organic matter-rich sediment (Rc/Ra = 0.02 and $\delta^{13}C\text{-}CO_2$ of $-30‰ \pm 10‰$ vs. V-PDB; Sano & Marty, 1995) and (d) limestone (Rc/Ra = 0.02 and $\delta^{13}C\text{-}CO_2$ of $0‰ \pm 2‰$ vs. V-PDB; Sano & Marty, 1995).

The gases from the central areas fall near the mixing line between a limestone component and an endogenous source, likely represented by the European Subcontinental Mantle. The peripheral areas show lower values of both Rc/Ra and $\delta^{13}C\text{-}CO_2$, although falling inside the field represented by the geothermal wells of Larderello (Gherardi et al., 2005), which are characterized by a mantle contribution up to 11.1% (Gherardi et al., 2005). Further information on the link between the peripheral areas and the Larderello geothermal system can be depicted in Figure 14b, where the gas samples are plotted on the CO_2–^3He–^4He ternary diagram (after Giggenbach et al., 1993). Here, mantle, air (1 Ra) and Air Saturated Water (ASW, 1 Ra) derived gases are also shown. As pointed out by Giggenbach et al. (1993), this diagram can be used to identify the loss and/or addition of specific volatile phases (e.g., CO_2, He) by linear trajectories on the plot. Gases from the central areas plot close to the CO_2 apex and have high $CO_2/^3He$ ratios (i.e., $>4.7 \times 10^{10}$), implying CO_2 and radiogenic ^4He addition in the hydrothermal system mostly derived from limestone and in agreement with the $\delta^{13}C\text{-}CO_2$ values (Minissale, 2004). On the contrary, Micciano, Montemiccioli, and Palazzo al Piano, along with the data from geothermal wells (Gherardi et al., 2005), show enrichment

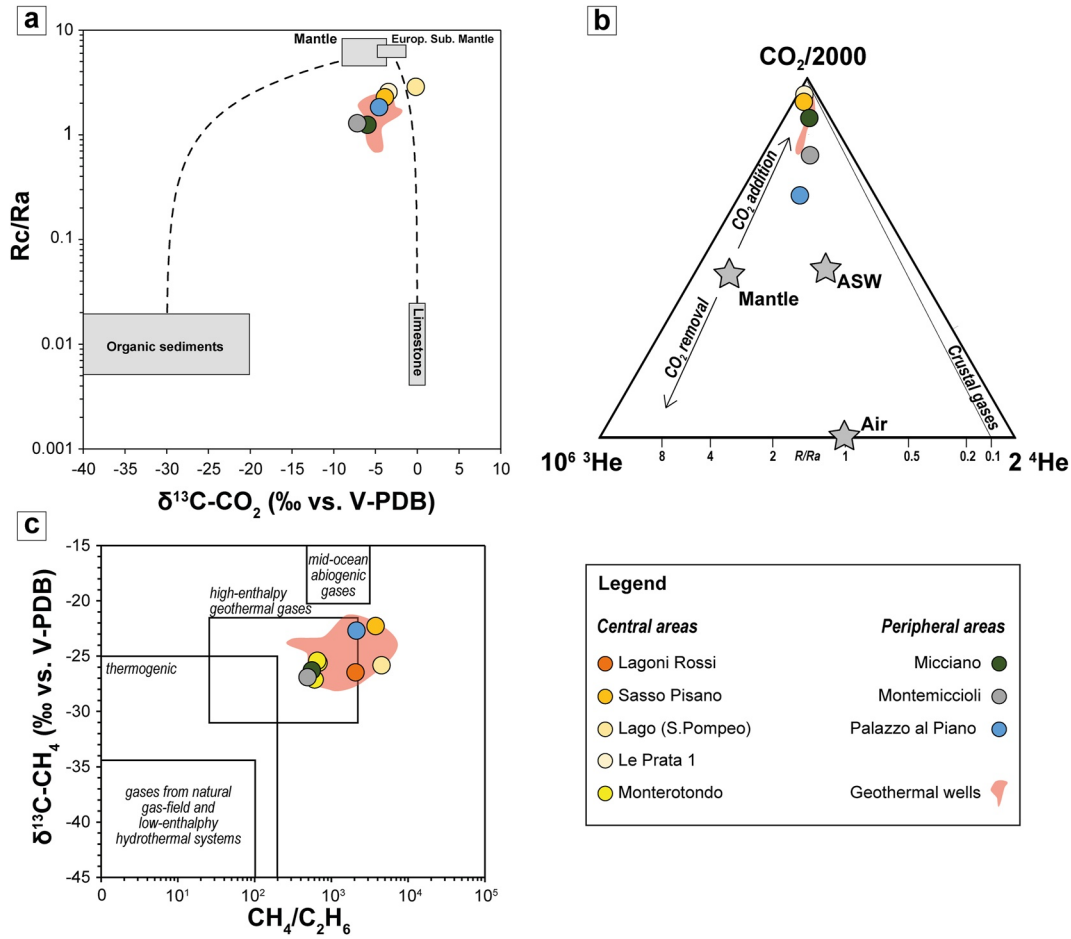

Figure 14. Plots of (a) δ^{13}C-CO_2 versus Rc/Ra; (b) CO_2–^{3}He–^{4}He ternary diagram; (c) δ^{13}C-CH_4 versus CH_4/C_2H_6. Gas data emitted from the main vent(s) in (a) and (b) are from Minissale (2004), while in (c) are from Tassi et al. (2012) and Venturi et al. (2019). Data from geothermal wells are from Gherardi et al. (2005).

in helium, plotting along a hypothetic line between Sasso Pisano and Le Prata 1 samples (Minissale, 2004) and the ASW, thus suggesting an interaction with a shallow aquifer. Noteworthy, Palazzo al Piano, which is located on the prosecution of a transfer zone that is parallel to the Larderello one, on which the Travale field is located (Figure 1), has the lowest $CO_2/^3$He ratio (7.4×10^9), indicating that the mantle contribution in this area is higher.

Eventually, the carbon isotopes of methane and the CH_4/C_2H_6 ratios also support a link between the gases discharged in the central areas and analyzed in the geothermal wells, and those in the peripheral areas. In Figure 14c, the δ^{13}C-CH_4 values (in ‰ vs. V-PDB) are plotted against the CH_4/C_2H_6 ratio (data from Tassi et al., 2012; Venturi et al., 2019; see Table S2 in Supporting Information S1). All samples show that the δ^{13}C-CH_4 values are between −27.1‰ and −22.3‰ versus V-PDB, with no evident differences between central and peripheral areas, and in the range of the δ^{13}C-CH_4 values of the geothermal reservoir (−28.0‰ and −21.4‰ vs. V-PDB; Gherardi et al., 2005), which, coupled with the CH_4/C_2H_6 ratios (from 603 to 4,347 and from 493 to 2,164 in the central and peripheral areas, respectively), support a common origin.

6. Concluding Remarks

Our study shows that at least 40 tons of CO_2 are released every day through both thermally active and cold-degassing hydrothermalized soils, located near the core and at the periphery of the Larderello geothermal system, respectively. Carbon dioxide emissions are strictly controlled by permeable sectors of the transfer faults, both along single fault segments or, mainly, at the intersection between these faults (NE-striking) and the normal faults (NW-striking) bounding the Pliocene-Quaternary structural depressions.

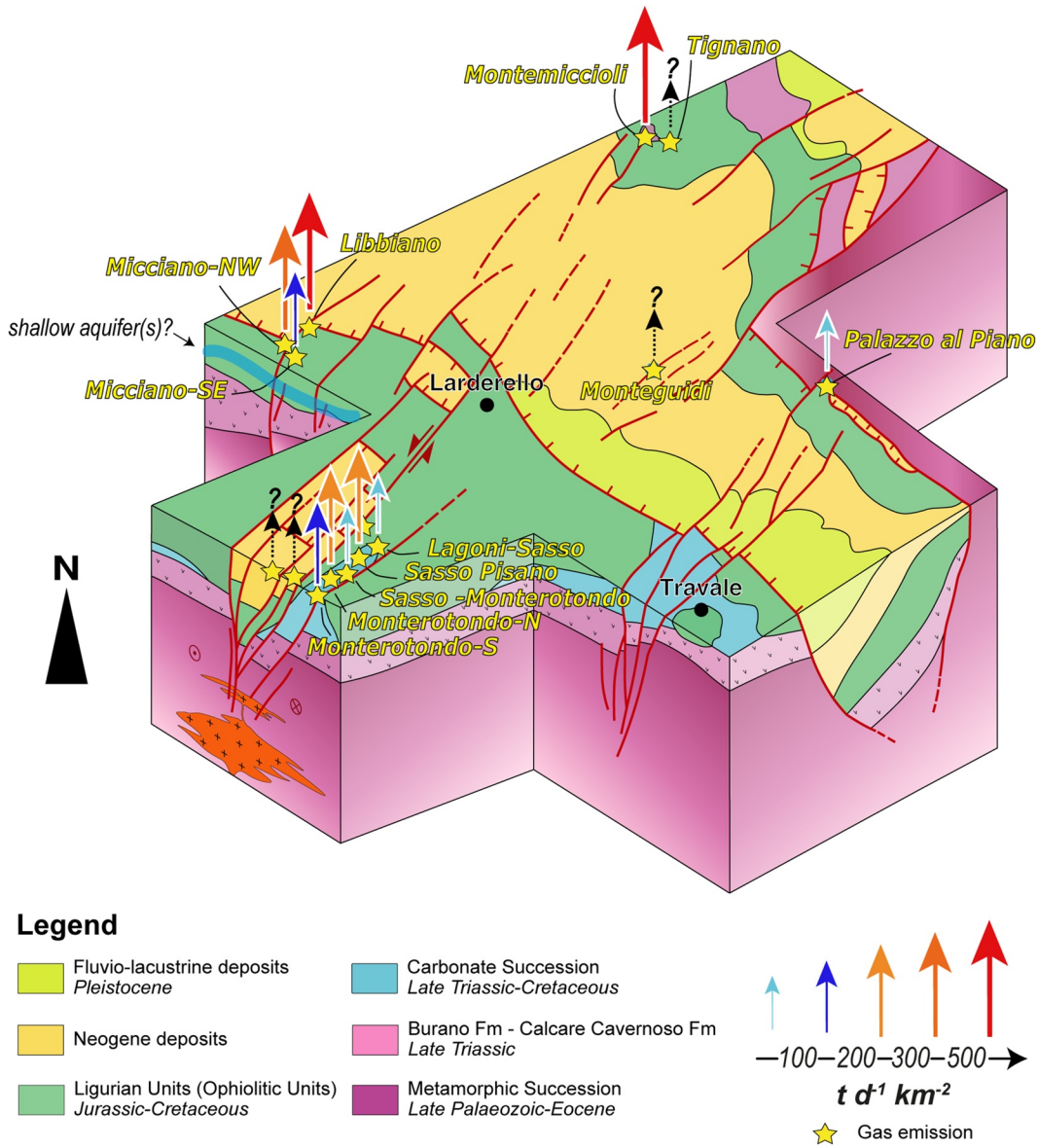

Figure 15. Geological sketch (not to scale) illustrating the tectonic context of the Larderello-Travale geothermal system. The main transfer zones and crustal faults driving the occurrence of the main geothermal manifestation in the area are highlighted. The spatial distribution of the normalized endogenous CO_2 diffuse emissions for the investigated sites is also reported.

The isotopic content of the interstitial CO_2 and the chemical and isotopic composition of the free gases emitted from the main vent(s) in the investigated areas supports a common deep origin among the central and peripheral zones, though different geochemical processes affect the CO_2 rising toward the surface. Central areas are characterized by CO_2 emissions accompanied by high amounts of steam and whose isotopic composition was affected by secondary processes that deeply modified the pristine isotopic composition. On the contrary, gases emitted from the peripheral areas were affected by strong condensation, although maintaining a general good correspondence of the isotopic fingerprint of the interstitial CO_2 with that of the CO_2 freely emitted from the main vent(s) occurring in these areas. This process enhances the release of important amount of diffuse CO_2, with higher rates of emission far from the core of the geothermal system, rather than in the central areas. All the CO_2 emission and geothermal manifestations related to the Larderello geothermal system are located along fault segments that are part of the transfer zone along which the geothermal area is developed, supporting its pivotal role in connecting the geothermal reservoir(s) with the surface and controlling the emission rates (Figure 15). This is particularly evident when the location of the hydrothermalized cold degassing areas is considered, especially that of

Montemiccioli (Figure 15). The latter shows the highest normalized emission rates of all the surveyed areas, with values comparable to those of some active volcanoes worldwide and occurs on the hypothetical continuation of the regional transfer zone that comprises the Lago basin, that is, the most efficient geothermal part of the Larderello production area. Carbon dioxide emissions in the southeastern peripheral area (i.e., Palazzo al Piano) are associated to a transfer zone that is parallel to the Larderello one, on which the Travale area is located (Figure 15).

In conclusion, the geochemical and structural features characterizing the peripheral areas suggest that the Larderello geothermal system might be wider than previously thought, indicating that further explorative studies should be carried out in the North and northeastern part of the area. This is also in agreement with the notable geothermal potential recognized in a zone located about 10 km North of Libbiano and Micciano localities by Bellani and Gherardi (2013).

Conflict of Interest

The authors declare no conflicts of interest relevant to this study.

Data Availability Statement

Carbon dioxide fluxes and carbon isotopic composition of the interstitial soil gases of this work can be found in Taussi et al. (2023). Carbon dioxide flux data from the Monterotondo-S area can be found in Cabassi et al. (2021). Carbon isotopic composition of the interstitial soil gases from the Monterotondo-S area can be found in Venturi et al. (2019). Data presented in Table S1 of the supplementary material are from Minissale (2004). Data presented in Table S2 of the supplementary material are from Tassi et al. (2012) and Venturi et al. (2019).

Acknowledgments

Many thanks are due to F. Tassi, M. Lazzaroni, and G. Morreale (University of Firenze), and A. Tempestilli (University of Urbino), for their assistance during the fieldwork in some of the Larderello areas. A. Lenzi (ENEL Green Power) provided the access in the Sasso Pisano-Monterotondo areas and guided us during the CO_2 flux measurements. This work was partially financially supported by the Laboratory of Stable Isotope Geochemistry of the Department of Earth Sciences (O.V.) and CNR-IGG (B.N.) of Florence. M.T. is thankful to A. Renzulli and University of Urbino for financial support through post-doc grants. M.Z. received funding from the Italian Ministry of University and Research (MIUR), through the program PON-AIM (Attraction and International Mobility)—project no. 1815472, Activity 1, line 1. The valuable comments and suggestions of A. Billi and an anonymous reviewer, who are sincerely thanked, helped us to improve the original manuscript. We are also thankful to the Editor-in-chief C. Faccenna for his editorial handling and suggestions.

References

Accaino, F., Tinivella, U., Rossi, G., & Nicolich, R. (2005). Imaging of CROP-18 deep seismic crustal data. *Bollettino- Societa Geologica Italiana*, *3*, 195–204.

Acocella, V., & Funiciello, R. (2006). Transverse systems along the extensional Tyrrhenian margin of central Italy and their influence on volcanism. *Tectonics*, *25*(2), TC2003. https://doi.org/10.1029/2005TC001845

Agostinetti, N. P., Licciardi, A., Piccinini, D., Mazzarini, F., Musumeci, G., Saccorotti, G., & Chiarabba, C. (2017). Discovering geothermal supercritical fluids: A new frontier for seismic exploration. *Scientific Reports*, *7*, 1–9.

Albarello, D., Batini, F., Bianciardi, P., Ciulli, B., Spinelli, E., & Viti, M. (2005). Stress field assessment from ill-defined fault plane solutions: An example from the Larderello geothermal field (western Tuscany, Italy). *Bollettino- Societa Geologica Italiana*, *3*, 187–193.

Alçiçek, H., Bülbül, A., Brogi, A., Liotta, D., Ruggieri, G., Capezzuoli, E., et al. (2018). Origin, evolution and geothermometry of the thermal waters in the Gölemezli geothermal field, Denizli Basin (SW Anatolia, Turkey). *Journal of Volcanology and Geothermal Research*, *349*, 1–30. https://doi.org/10.1016/j.jvolgeores.2017.07.021

Alçiçek, M. C., Brogi, A., Capezzuoli, E., Liotta, D., & Meccheri, M. (2013). Superimposed basins formation during the Neogene–Quaternary extensional tectonics in SW Anatolia (Turkey): Insights from the kinematics of the Dinar fault zone. *Tectonophysics*, *608*, 713–727. https://doi.org/10.1016/j.tecto.2013.08.008

Allis, R. G. (1981). Changes in heat flow associated with exploitation of Wairakei Geothermal Field, New Zealand. *New Zealand Journal of Geology and Geophysics*, *24*(1), 1–19. https://doi.org/10.1080/00288306.1981.10422694

Anderson, T. R., & Fairley, J. P. (2008). Relating permeability to the structural setting of a fault-controlled hydrothermal system in southeast Oregon, USA. *Journal of Geophysical Research*, *113*(B5), B05402. https://doi.org/10.1029/2007jb004962

Bagagli, M., Kissling, E., Piccinini, D., & Saccorotti, G. (2020). Local earthquake tomography of the Larderello-Travale geothermal field. *Geothermics*, *83*, 101731. https://doi.org/10.1016/j.geothermics.2019.101731

Bally, A. W. (1981). Atlantic type margins in geology of passive continental margins: History, structure and sedimentologic record. In *AAPG Education Course Notes Series* (Vol. 19, pp. 1–48).

Barbier, E. (2002). Geothermal energy technology and current status: An overview. *Renewable & Sustainable Energy Reviews*, *6*(1–2), 3–65. https://doi.org/10.1016/s1364-0321(02)00002-3

Barchi, M. R. (2010). The neogene-quaternary evolution of the Northern Apennines: Crustal structure, style of deformation and seismicity. In M. Beltrando, A. Peccerillo, M. Mattei, S. Conticelli, & C. Doglioni (Eds.), *The Neogene-quaternary evolution of the Northern Apennines: Crustal structure, style of deformation* (Vol. 36). https://doi.org/10.3809/jvirtex.2009.00220

Bartole, R. (1995). The North-Tyrrhenian–Northern Apennines post-collisional system: Constraints for a geodynamic model. *Terra Nova*, *1*, 7–30. https://doi.org/10.1111/j.1365-3121.1995.tb00664.x

Batini, F., Bertini, G., Giannelli, G., Pandeli, E., & Puxeddu, M. (1983). Deep structure of the Larderello geothermal field: Contribution from recent geophysical and geological data. *Memorie della Societa Geologica Italiana*, *5*, 219–235.

Batini, F., Brogi, A., Lazzarotto, A., Liotta, D., & Pandeli, E. (2003). Geological features of Larderello-Travale and Mt. Amiata geothermal areas (southern Tuscany, Italy). *Episodes*, *26*(3), 239–244. https://doi.org/10.18814/epiiugs/2003/v26i3/015

Batini, F., Burgassi, P. D., Cameli, G. M., Nicolich, R., & Squarci, P. (1978). Contribution to the study of the deep lithospheric profiles: Deep reflecting horizons in Larderello-Travale geothermal field. *Memorie della Societa Geologica Italiana*, *19*, 477–484.

Bellani, S., & Gherardi, F. (2013). Thermal overview of an area NW of the Larderello geothermal field, Italy. *Transactions Geothermal Resources Council*, *37*, 231–235.

Bertani, R., Bertini, G., Cappetti, G., Fiordelisi, A., & Marocco, B. M. (2005). An update of the Larderello-Travale/Radicondoli deep geothermal system proceedings of the World Geothermal congress (pp. 24–29).
Bertani, R., Parisi, L., Perini, R., & Tarquini, B. (1999). High-temperature measurements of water adsorption in geothermal rocks. *Geothermics*, *28*(2), 277–294. https://doi.org/10.1016/s0375-6505(99)00008-5
Bertani, R., & Thain, I. (2002). *Geothermal power generating plant CO_2 emission survey* (Vol. 49, pp. 1–3). IGA News.
Bertini, G., Casini, M., Gianelli, G., & Pandeli, E. (2006). Geological structure of a long-living geothermal system, Larderello. Italy. *Terra Nova*, *18*(3), 163–169. https://doi.org/10.1111/j.1365-3121.2006.00676.x
Bianco, C., Brogi, A., Caggianelli, A., Giorgetti, G., Liotta, D., & Meccheri, M. (2015). HP-LT metamorphism in Elba Island: Implications for the geodynamic evolution of the inner Northern Apennines (Italy). *Journal of Geodynamics*, *91*, 13–25. https://doi.org/10.1016/j.jog.2015.08.001
Bianco, C., Godard, G., Halton, A., Brogi, A., Liotta, D., & Caggianelli, A. (2019). The lawsonite-glaucophane blueschists of Elba Island (Italy). *Lithos*, *348–349*, 105198. https://doi.org/10.1016/j.lithos.2019.105198
Bolognesi, L. (2011). The oxygen isotope exchange between carbon dioxide and water in the Larderello geothermal field (Italy) during fluid reinjection. *Geothermics*, *40*(3), 181–189. https://doi.org/10.1016/j.geothermics.2011.06.002
Brogi, A. (2020). Late evolution of the inner Northern Apennines from the structure of the Monti del Chianti-Monte Cetona ridge (Tuscany, Italy). *Journal of Structural Geology*, *141*, 104205. https://doi.org/10.1016/j.jsg.2020.104205
Brogi, A., Caggianelli, A., Liotta, D., Zucchi, M., Spina, A., Capezzuoli, E., et al. (2021). The Gavorrano monzogranite (Northern Apennines): An updated review of host rock protoliths, thermal metamorphism and tectonic setting. *Geosciences*, *11*(3), 124. https://doi.org/10.3390/geosciences11030124
Brogi, A., Fidolini, F., & Liotta, D. (2013). Tectonic and sedimentary evolution of the upper Valdarno Basin: New insights from the lacustrine S. Barbara Basin. *Italian Journal of Geoscience*, *132*(1), 81–97. https://doi.org/10.3301/ijg.2012.08
Brogi, A., & Giorgetti, G. (2012). Tectono-metamorphic evolution of the siliciclastic units in the Middle Tuscan range (inner Northern Apennines): Mg-Carpholite bearing quartz veins related to syn-metamorphic syn-orogenic foliation. *Tectonophysics*, *526–529*, 167–184. https://doi.org/10.1016/j.tecto.2011.09.015
Brogi, A., Lazzarotto, A., & Liotta, D., & CROP-18 Working Group. (2005). Structural features of southern Tuscany and geological interpretation of the CROP 18 seismic reflection survey (Italy). *Bollettino Società Geologica Italiana*, *3*, 213–236.
Brogi, A., & Liotta, D. (2008). Highly extended terrains, lateral segmentation of the substratum, and basin development: The Middle–late Miocene Radicondoli Basin (inner northern Apennines, Italy). *Tectonics*, *27*(5), TC5002. https://doi.org/10.1029/2007tc002188
Brogi, A., Liotta, D., Capezzuoli, E., Matera, P. F., Kele, S., Soligo, M., et al. (2020). Travertine deposits constraining transfer zone neotectonics in geothermal areas: An example from the inner Northern Apennines (Bagno Vignoni-Val d'Orcia area, Italy). *Geothermics*, *85*, 101763. https://doi.org/10.1016/j.geothermics.2019.101763
Brunet, C., Monie, P., Jolivet, L., & Cadet, J. P. (2000). Migration of compression and extension in the Tyrrhenian sea, insights from $^{40}Ar/^{39}Ar$ ages on micas along a transect from Corsica to Tuscany. *Tectonophysics*, *321*(1), 127–155. https://doi.org/10.1016/s0040-1951(00)00067-6
Cabassi, J., Venturi, S., Di Bennardo, F., Nisi, B., Tassi, F., Magi, F., et al. (2021). Flux measurements of gaseous elemental mercury (GEM) from the geothermal area of "Le Biancane" natural park (Monterotondo Marittimo, Grosseto, Italy): Biogeochemical processes controlling GEM emission. *Journal of Geochemical Exploration*, *228*, 106824. https://doi.org/10.1016/j.gexplo.2021.106824
Caine, J. S., Evans, I. P., & Forster, C. B. (1996). Fault zone architecture and permeability structure. *Geology*, *24*(11), 1025–1028. https://doi.org/10.1130/0091-7613(1996)024<1025:fzaaps>2.3.co;2
Calcagnile, G., & Panza, G. F. (1981). The main characteristics of the lithosphere–astenosphere system in Italy and surrounding regions. *Pure and Applied Geophysics*, *119*(4), 865–879. https://doi.org/10.1007/bf01131263
Camarda, M., De Gregorio, S., Capasso, G., Di Martino, R. M. R., Gurrieri, G., & Prano, V. (2019). The monitoring of natural soil CO_2 emissions: Issues and perspectives. *Earth-Science Reviews*, *198*, 102928. https://doi.org/10.1016/j.earscirev.2019.102928
Camarda, M., De Gregorio, S., Favara, R., & Gurrieri, S. (2007). Evaluation of carbon isotope fractionation of soil CO_2 under an advective–diffusive regimen: A tool for computing the isotopic composition of unfractionated deep source. *Geochimica et Cosmochimica Acta*, *71*(12), 3016–3027. https://doi.org/10.1016/j.gca.2007.04.002
Camarda, M., Gurrieri, S., & Valenza, M. (2006). CO_2 flux measurements in volcanic areas using the dynamic concentration method: Influence of soil permeability. *Journal of Geophysical Research*, *111*(B5), B05202. https://doi.org/10.1029/2005jb003898
Cameli, G. M., Dini, I., & Liotta, D. (1993). Upper crustal structure of the Larderello geothermal field as a feature of post collisional extensional tectonics (Southern Tuscany, Italy). *Tectonophysics*, *224*(4), 413–423. https://doi.org/10.1016/0040-1951(93)90041-h
Cameli, G. M., Dini, I., & Liotta, D. (1998). Brittle/ductile boundary from seismic reflection lines of southern Tuscany (Northern Apennines, Italy). *Memorie della Societa Geologica Italiana*, *52*, 153–163.
Capasso, G., D'Alessandro, W., Favara, R., Inguaggiato, S., & Parello, F. (2001). Kinetic isotope fractionation of CO_2 carbon due to diffusion processes through the soil. In R. Cidu (Ed.), *Proceeding of the 10th international symposium water-rock interaction* (pp. 1497–1499).
Carapezza, M. L., Ranaldi, M., Gattuso, A., Pagliuca, N. M., & Tarchini, L. (2015). The sealing capacity of the cap rock above the Torre Alfina geothermal reservoir (Central Italy) revealed by soil CO_2 flux investigations. *Journal of Volcanology and Geothermal Research*, *291*, 25–34. https://doi.org/10.1016/j.jvolgeores.2014.12.011
Cardellini, C., Chiodini, G., & Frondini, F. (2003). Application of stochastic simulation to CO_2 flux from soil: Mapping and quantification of gas release. *Journal of Geophysical Research*, *108*(B9), 2425.
Carmignani, L., Decandia, F. A., Disperati, L., Fantozzi, P. L., Kligfield, R., Lazzarotto, A., et al. (2001). Inner Northern Apennines. In G. B. Vai & I. P. Martini (Eds.), *Anatomy of an orogen: The Apennines and adjacent mediterranean basins*. Kluwer.
Carmignani, L., Decandia, F. A., Disperati, L., Fantozzi, P. L., Lazzarotto, A., Liotta, D., & Oggiano, G. (1995). Relationships between the Sardinia–Corsica–Provencal domain and the Northern Apennines. *Terra Nova*, *7*(2), 128–137. https://doi.org/10.1111/j.1365-3121.1995.tb00681.x
Ceccarelli, A., Celati, R., Grassi, S., & Minissale, A. (1985). Interaction between vapour-dominated reservoirs and surrounding aquifers: The case of the southern boundary of Larderello field. In *Proceeding of the international symposium on geothermal energy* (Vol. 9, pp. 267–272).
Chiodini, G., Baldini, A., Barberi, F., Carapezza, M. L., Cardellini, C., Frondini, F., et al. (2007). Carbon dioxide degassing at Latera caldera (Italy): Evidence of geothermal reservoir and evaluation of its potential energy. *Journal of Geophysical Research*, *112*(B12), B12204. https://doi.org/10.1029/2006jb004896
Chiodini, G., Caliro, S., Cardellini, C., Avino, R., Granieri, D., & Schmidt, A. (2008). Carbon isotopic composition of soil CO_2 efflux, a powerful method to discriminate different sources feeding soil CO_2 degassing in volcanic-hydrothermal areas. *Earth and Planetary Science Letters*, *274*(3–4), 372–379. https://doi.org/10.1016/j.epsl.2008.07.051
Chiodini, G., Cioni, R., Guidi, M., Raco, B., & Marini, L. (1998). Soil CO_2 flux measurements in volcanic and geothermal areas. *Applied Geochemistry*, *13*(5), 543–552. https://doi.org/10.1016/s0883-2927(97)00076-0

Costantini, A., Lazzarotto, A., Liotta, D., Mazzanti, R., Mazzei, R., & Salvatorini, G. (2002). *Note illustrative Della Carta Geologica d'Italia Alla Scala 1:50.000-Foglio 306 Massa Marittima* (p. 172). L.A.C.

Cox, S. F., Knackstedt, M. A., & Braun, J. (2001). Principles of structural control on perme-ability and fluid flow in hydrothermal systems. *Reviews in Economic Geology*, *11*, 1–24.

Craig, H. (1963). The isotope geochemistry of water and carbon in geothermal areas. In E. Tongiorgi (Ed.), *Nuclear geology on geothermal areas. Proceeding of the international symposium* (pp. 17–54).

Curewitz, D., & Karson, J. A. (1997). Structural settings of hydrothermal outflow: Fracture permeability maintained by fault propagation and interaction. *Journal of Volcanology and Geothermal Research*, *79*(3–4), 149–168. https://doi.org/10.1016/s0377-0273(97)00027-9

D'Alessandro, W., Giammanco, S., Parello, F., & Valenza, M. (1997). CO_2 output and $\delta^{13}C(CO_2)$ from Mount Etna as indicators of degassing of shallow asthenosphere. *Bulletin of Volcanology*, *58*(6), 455–458. https://doi.org/10.1007/s004450050154

Dallmeyer, R. D., & Liotta, D. (1998). Extension, uplift of rocks and cooling ages in thinned crustal provinces: The Larderello geothermal Area (Inner Northern Apennines, Italy). *Geological Magazine*, *135*(2), 193–202. https://doi.org/10.1017/s0016756898008309

D'Amore, F., & Truesdell, A. (1984). Helium in the Larderello geothermal fluid. *Geothermics*, *13*(3), 227–239. https://doi.org/10.1016/0375-6505(84)90018-x

David, M. (1977). *Geostatistical ore Reserve estimation* (p. 384). Elsevier Science.

De Franco, R., Petracchini, L., Scrocca, D., Caielli, G., Montegrossi, G., Santilano, A., & Manzella, A. (2019). Synthetic seismic reflection modelling in a supercritical geothermal system: An Image of the K-horizon in the Larderello field (Italy). *Geofluids*, *2019*, 1–21. https://doi.org/10.1155/2019/8492453

Della Vedova, B., Bellani, S., Pellis, G., & Squarci, P. (2001). Deep temperatures and surface heat flow distribution. In G. B. Vai & I. P. Martini (Eds.), *Anatomy of an orogeny: The Apennines and adjacent Mediterranean basins* (pp. 65–76). Kluwer Academic Publishers.

De Matteis, R., Vanorio, T., Zollo, A., Ciuffi, S., Fiordelisi, A., & Spinelli, E. (2008). Three-dimensional tomography and rock properties of the Larderello-Travale geothermal area. Italy. *Physics of the Earth and Planetary Interiors*, *168*(1–2), 37–48. https://doi.org/10.1016/j.pepi.2008.04.019

Dini, A., Gianelli, G., Puxeddu, M., & Ruggieri, G. (2005). Origin and evolution of pliocene-pleistocene granites from the Larderello geothermal field (Tuscan magmatic province, Italy). *Lithos*, *81*(1–4), 1–31. https://doi.org/10.1016/j.lithos.2004.09.002

Dini, A., Westerman, D. S., Innocenti, F., & Rocchi, S. (2008). Magma emplacement in a transfer zone: The Miocene mafic Orano dyke swarm of Elba Island, Tuscany, Italy. *Geological Society, London, Special Publications*, *302*(1), 131–148. https://doi.org/10.1144/sp302.10

Di Stefano, R., Bianchi, I., Ciaccio, M. G., Carrara, G., & Kissling, E. (2011). Three-dimensional Moho topography in Italy: New constraints from receiver functions and controlled source seismology. *Geochemistry, Geophisics, Geosystems*, *12*(9), Q09006. https://doi.org/10.1029/2011gc003649

Duchi, V., Minissale, A. A., & Manganelli, M. (1992). Chemical composition of natural deep and shallow hydrothermal fluids in the Larderello geothermal field. *Journal of Volcanology and Geothermal Research*, *49*(3–4), 313–328. https://doi.org/10.1016/0377-0273(92)90020-e

Dunai, T. J., & Baur, H. (1985). Helium, neon, and argon systematics of the European subcontinental mantle: Implications for its geochemical evolution. *Geochimica et Cosmochimica Acta*, *59*(13), 2767–2783. https://doi.org/10.1016/0016-7037(95)00172-v

Elter, M., & Pandeli, E. (1990). Alpine and Variscan orogenic phases in the basement rocks of the Northern Apennines (Larderello geothermal field, southern Tuscany, Italy). *Eclogae Geologicae Helvetiae*, *83*, 241–264.

Farina, F., Dini, A., Davies, J. H. F. L., Ovtcharova, M., Greber, N. D., Bouvier, A.-S., et al. (2018). Zircon petrochronology reveals the timescale and mechanism of anatectic magma formation. *Earth and Planetary Science Letters*, *495*, 213–223. https://doi.org/10.1016/j.epsl.2018.05.021

Faulds, J. E., Hinz, N., Kreemer, C., & Coolbaugh, M. (2012). Regional patterns of geothermal activity in the Great Basin region, western USA: Correlation with strain rates. *Transactions Geothermal Resources Council*, *36*(2), 897–902.

Faulds, J. E., & Varga, R. J. (1998). The role of the accommodation zones and transfer zones in the regional segmentation of extended terranes. In J. E. Faulds & J. H. Stewart (Eds.), *Accommodation zones and transfer zones; the regional segmentation of the basin and range province, GSA special papers*.

Faulkner, D. R., & Armitage, P. J. (2013). The effect of tectonic environment on permeability development around faults and in the brittle crust. *Earth and Planetary Science Letters*, *375*, 71–77. https://doi.org/10.1016/j.epsl.2013.05.006

Faulkner, D. R., Jackson, C. a. L., Lunn, R. J., Schlische, R. W., Shipton, Z. K., Wibberley, C. A. J., & Withjack, M. O. (2010). A review of recent developments concerning the structure, mechanics and fluid flow properties of fault zones. *Journal of Structural Geology*, *32*(11), 1557–1575. https://doi.org/10.1016/j.jsg.2010.06.009

Federico, C., Corso, P. P., Fiordilino, E., Cardellini, C., Chiodini, G., Parello, F., & Pisciotta, A. (2010). CO_2 degassing at La Solfatara volcano (Phlegrean Fields): Processes affecting $\delta^{13}C$ and $\delta^{18}O$ of soil CO_2. *Geochimica et Cosmochimica Acta*, *74*(12), 3521–3538. https://doi.org/10.1016/j.gca.2010.03.010

Ferrara, G. C., Gonfiantini, R., & Panichi, C. (1965). La composizione isotopica del vapore dl alcuni soffioni di Larderello e dell'acqua di alcune sorgenti e mofete della Toscana. *Atti Società Toscana Scienze Naturali-Seria A*, *72*, 3–21.

Fischer, T. P., Arellano, S., Carn, S., Aiuppa, A., Galle, B., Allard, P., et al. (2019). The emissions of CO_2 and other volatiles from the world's subaerial volcanoes. *Scientific Reports*, *9*(1), 18716. https://doi.org/10.1038/s41598-019-54682-1

Foley, l. E., Toksoz, M. N., & Batini, F. (1992). Inversion of teleseismic traveltime residuals for velocity structure in the Larderello geothermal field. Italy. *Geophysical Research Letters*, *19*(1), 5–8. https://doi.org/10.1029/91gl01182

Fridriksson, T., Kristjánsson, B. R., Ármannsson, H., Margrétardóttir, E., Ólafsdóttir, S., & Chiodini, G. (2006). CO_2 emissions and heat flow through soil, fumaroles, and steam heated mud pools at the Reykjanes geothermal area, SW Iceland. *Applied Geochemistry*, *21*(9), 1551–91569. https://doi.org/10.1016/j.apgeochem.2006.04.006

Fridriksson, T., Mateos Merino, A., Yasemin Orucu, A., & Audinet, P. (2017). Greenhouse gas emissions from geothermal power production. In *Proceedings, 42nd workshop on geothermal reservoir engineering* (pp. 13–15). Stanford University.

Frondini, F., Caliro, S., Cardellini, C., Chiodini, G., & Morgantini, N. (2009). Carbon dioxide degassing and thermal energy release in the Monte Amiata volcanic-geothermal area (Italy). *Applied Geochemistry*, *24*(5), 860–875. https://doi.org/10.1016/j.apgeochem.2009.01.010

Ganerød, G. V., Braathen, A., & Willemoes-Wissing, B. (2008). Predictive permeability model of extensional faults in crystalline and metamorphic rocks; verification by pre-grouting in two sub-sea tunnels, Norway. *Journal of Structural Geology*, *30*(8), 993–1004. https://doi.org/10.1016/j.jsg.2008.04.001

Gautheron, C., Moreira, M., & Allègre, C. (2005). He, Ne and Ar composition of the European lithospheric mantle. *Chemical Geology*, *217*(1–2), 97–112. https://doi.org/10.1016/j.chemgeo.2004.12.009

Gherardi, F., Panichi, C., Gonfiantini, R., Magro, G., & Scandiffio, G. (2005). Isotope systematics of C-bearing gas compounds in the geothermal fluids of Larderello, Italy. *Geothermics*, *34*(4), 442–470. https://doi.org/10.1016/j.geothermics.2004.09.005

Giammanco, S., Gurrieri, S., & Valenza, M. (1997). Soil CO_2 degassing along tectonic structures of mount Etna (Sicily): The Pernicana fault. *Applied Geochemistry*, *12*(4), 429–436. https://doi.org/10.1016/s0883-2927(97)00011-5

Gianelli, G., Ruggieri, G., & Mussi, M. (1997). Isotopic and fluid inclusion study of hydrothermal and metamorphic carbonates in the Larderello geothermal field and surrounding areas, Italy. *Geothermics*, *26*(3), 393–417. https://doi.org/10.1016/s0375-6505(97)00001-1

Gibbs, A. D. (1984). Structural evolution of extensional basin margins. *Journal of the Geological Society of London*, *141*(4), 609–620. https://doi.org/10.1144/gsjgs.141.4.0609

Gibbs, A. D. (1990). Linked fault families in basin formation. *Journal of Structural Geology*, *12*(5–6), 795–803. https://doi.org/10.1016/0191-8141(90)90090-l

Giggenbach, W., Sano, Y., & Wakita, H. (1993). Isotopic composition of helium, and CO_2 and CH_4, contents in gases produced along the New Zealand part of a convergent plate boundary. *Geochimica et Cosmochimica Acta*, *57*(14), 3427–3455. https://doi.org/10.1016/0016-7037(93)90549-c

Giuntoli, F., & Viola, G. (2021). Cyclic brittle-ductile oscillations recorded in exhumed high-pressure continental units: A record of deep episodic tremor and slow slip events in the Northern Apennines. *Geochemistry, Geophysics, Geosystems*, *22*(9), e2021GC009805. https://doi.org/10.1029/2021gc009805

Gola, G., Bertini, G., Bonini, M., Botteghi, S., Brogi, A., De Franco, R., et al. (2017). Data integration and conceptual modelling of the Larderello geothermal area. Italy. *Energy Procedia*, *125*, 300–309. https://doi.org/10.1016/j.egypro.2017.08.201

Granieri, D., Mazzarini, F., Cerminara, M., Calusi, B., Scozzari, A., Menichini, M., & Lelli, M. (2023). Shallow portion of an active geothermal system revealed by multidisciplinary studies: The case of Le Biancane (Larderello, Italy). *Geothermics*, *108*, 102616. https://doi.org/10.1016/j.geothermics.2022.102616

Hooker, P. J., Bertrami, R., Lombardi, S., O'Nions, R. K., & Oxburgh, E. R. (1985). Helium-3 anomalies and crust-mantle interaction in Italy. *Geochimica et Cosmochimica Acta*, *49*(12), 2505–2513. https://doi.org/10.1016/0016-7037(85)90118-8

Inguaggiato, C., Vita, F., Diliberto, I. S., & Calderone, L. (2017). The role of the aquifer in soil CO_2 degassing in volcanic peripheral areas: A case study of Stromboli Island (Italy). *Chemical Geology*, *469*, 110–116. https://doi.org/10.1016/j.chemgeo.2016.12.017

Inguaggiato, S., Jácome Paz, M. P., Mazot, A., Delgado Granados, H., Inguaggiato, C., & Vita, F. (2013). CO_2 output discharged from Stromboli Island (Italy). *Chemical Geology*, *339*, 52–60. https://doi.org/10.1016/j.chemgeo.2012.10.008

Jentsch, A., Duesing, W., Jolie, E., & Zimmer, M. (2021). Monitoring the response of volcanic CO_2 emissions to changes in the Los Humeros hydrothermal system. *Scientific Reports*, *11*(1), 17972. https://doi.org/10.1038/s41598-021-97023-x

Jentsch, A., Jolie, E., Jones, D. G., Taylor-Curran, H., Peiffer, L., Zimmer, M., & Lister, B. (2020). Magmatic volatiles to assess permeable volcano-tectonic structures in the Los Humeros geothermal field. Mexico. *Journal of Volcanology and Geothermal Research*, *394*, 106820. https://doi.org/10.1016/j.jvolgeores.2020.106820

Jolie, E., Hutchison, W., Driba, D. L., Jentsch, A., & Gizaw, B. (2019). Pinpointing deep geothermal upflow in zones of complex tectono-volcanic degassing: New insights from Aluto volcano, Main Ethiopian Rift. *Geochemistry, Geophysics, Geosystems*, *20*(8), 4146–4161. https://doi.org/10.1029/2019gc008309

Jolie, E., Klinkmueller, M., Moeck, I., & Bruhn, D. (2016). Linking gas fluxes at Earth's surface with fracture zones in an active geothermal field. *Geology*, *44*(3), 187–190. https://doi.org/10.1130/g37412.1

Jung, N.-H., Han, W. S., Watson, Z. T., Graham, J. P., & Kim, K.-Y. (2014). Fault-controlled CO_2 leakage from natural reservoirs in the Colorado Plateau, East-Central Utah. *Earth and Planetary Science Letters*, *403*, 358–367. https://doi.org/10.1016/j.epsl.2014.07.012

Kaya, E., & Zarrouk, S. J. (2017). Reinjection of greenhouse gases into geothermal reservoirs. *International Journal of Greenhouse Gas Control*, *67*, 111–129. https://doi.org/10.1016/j.ijggc.2017.10.015

Klusman, R. W., Moore, J. N., & LeRoy, M. (2000). Potential for surface gas flux measurements in exploration and surface evaluation of geothermal resources. *Geothermics*, *29*(6), 637–370. https://doi.org/10.1016/s0375-6505(00)00036-5

Lamberti, M. C., Agusto, A., Llano, J., Nogués, V., Venturi, S., Vélez, M. L., et al. (2021). Soil CO_2 flux baseline in Plancóhn–Peteroa volcanic complex, southern Andes, Argentina–Chile. *Journal of South American Earth Sciences*, *105*, 102930. https://doi.org/10.1016/j.jsames.2020.102930

Lazzarotto, A. (1967). Geologia della zona compresa fra l'alta valle del Fiume Cornia ed il torrente Pavone (provincia di Pisa e Grosseto). *Memorie della Societa Geologica Italiana*, *6*, 151–197.

Lazzarotto, A., & Mazzanti, R. (1978). Geologia dell'alta val di Cecina. *Bollettino della Societa Geologica Italiana*, *95*, 1365–1487.

Leila, M., Lévy, D., Battani, A., Piccardi, L., Šegvić, B., Badurina, L., et al. (2021). Origin of continuous hydrogen flux in gas manifestations at the Larderello geothermal field, Central Italy. *Chemical Geology*, *585*, 120564. https://doi.org/10.1016/j.chemgeo.2021.120564

Lelli, M., & Raco, B. (2017). A reliable and effective methodology to monitor CO_2 flux from soil: The case of Lipari Island (Sicily, Italy). *Applied Geochemistry*, *85*, 73–85. https://doi.org/10.1016/j.apgeochem.2017.08.004

Lenzi, A., Paci, M., Giudetti, G., & Gambini, R. (2021). Tracing ancient carbon dioxide emission in the larderello area by means of historical boric acid production data. *Energies*, *14*, 4101. https://doi.org/10.3390/en14144101

Liotta, D. (1991). The Arbia-Val Marecchia line, Northern Apennines. *Eclogae Geologicae Helvetiae*, *84*, 413–430.

Liotta, D., & Brogi, A. (2020). Pliocene-Quaternary fault kinematics in the Larderello geothermal area (Italy): Insights for the interpretation of the present stress field. *Geothermics*, *83*, 101714. https://doi.org/10.1016/j.geothermics.2019.101714

Liotta, D., Brogi, A., Meccheri, M., Dini, A., Bianco, C., & Ruggieri, G. (2015). Coexistence of low-angle normal and high-angle strike- to oblique-slip faults during Late Miocene mineralization in eastern Elba Island (Italy). *Tectonophysics*, *660*, 17–34. https://doi.org/10.1016/j.tecto.2015.06.025

Liotta, D., Brogi, A., Ruggieri, G., & Zucchi, M. (2021). Fossil vs. active geothermal systems: A field and laboratory method to disclose the relationships between geothermal fluid flow and geological structures at depth. *Energies*, *14*(4), 933. https://doi.org/10.3390/en14040933

Liotta, D., & Ranalli, G. (1999). Correlation between seismic reflectivity and rheology in extended lithosphere: Southern Tuscany, Inner Northern Apennines. Italy. *Tectonophysics*, *315*(1–4), 109–122. https://doi.org/10.1016/s0040-1951(99)00292-9

Li Vigni, L., Cardellini, C., Temovski, M., Ionescu, A., Molnár, K., Palcsu, L., et al. (2022). Duvalo "volcano" (North Macedonia): A purely tectonic-related CO_2 degassing system. *Geochemistry, Geophysics, Geosystems*, *23*(4), e2021GC010198. https://doi.org/10.1029/2021gc010198

Magro, G., Ruggieri, G., Gianelli, G., Bellani, S., & Scandiffio, G. (2003). Helium isotopes in paleofluids and present-day fluids of the Larderello geothermal field: Constraints on the heat source. *Journal of Geophysical Research*, *108*(B1), ECV3-12. https://doi.org/10.1029/2001jb001590

Manzella, A. (2004). Resistivity and heterogeneity of Earth crust in an active tectonic region, Southern Tuscany (Italy). *Annals of Geophysics*, *47*, 107–118.

Manzella, A., Bonciani, R., Allansdottir, A., Botteghi, S., Donato, A., Giamberini, S., et al. (2018). Environmental and social aspects of geothermal energy in Italy. *Geothermics*, *72*, 232–248. https://doi.org/10.1016/j.geothermics.2017.11.015

Mariucci, M. T., Amato, A., & Montone, P. (1999). Recent tectonic evolution and present stress in the Northern Apennines (Italy). *Tectonics*, *18*(1), 108–118. https://doi.org/10.1029/1998tc900019

Mariucci, M. T., & Montone, P. (2020). Database of Italian present-day stress indicators, IPSI 1.4. *Scientific Data*, *7*(1), 298. https://doi.org/10.1038/s41597-020-00640-w

Martini, I. P., & Sagri, M. (1993). Tectono-sedimentary characteristics of Late Miocene-Quaternary extensional basins of the Northern Apennines, Italy. *Earth-Science Reviews*, *34*(3), 197–233. https://doi.org/10.1016/0012-8252(93)90034-5

Mason, E., Edmonds, M., & Turchyn, A. V. (2017). Remobilization of crustal carbon may dominate volcanic arc emissions. *Science*, *357*(6348), 290–294. https://doi.org/10.1126/science.aan5049

Miao, Q., Xu, C., Hao, F., Yin, J., Wang, Q., Xie, M., et al. (2020). Roles of fault structures on the distribution of mantle-derived CO_2 in the Bohai Bay basin, NE China. *Journal of Asian Earth Sciences*, *197*, 104398. https://doi.org/10.1016/j.jseaes.2020.104398

Minissale, A. (1991). The Larderello geothermal field: A review. *Earth Sciences Reviews*, *31*(2), 133–151. https://doi.org/10.1016/0012-8252(91)90018-b

Minissale, A. (2004). Origin, transport and discharge of CO_2 in central Italy. *Earth-Science Reviews*, *66*(1–2), 89–141. https://doi.org/10.1016/j.earscirev.2003.09.001

Minissale, A. (2018). A simple geochemical prospecting method for geothermal resources in flat areas. *Geothermics*, *72*, 258–267. https://doi.org/10.1016/j.geothermics.2017.12.001

Minissale, A., Evans, W. C., Magro, G., & Vaselli, O. (1997). Multiple source components in gas manifestations from north-central Italy. *Chemical Geology*, *142*(3–4), 175–192. https://doi.org/10.1016/s0009-2541(97)00081-8

Óladóttir, A. A., & Fridriksson, T. (2015). The evolution of CO_2 emissions and heat flow through soil since 2004 in the utilized Reykjanes geothermal Area, SW Iceland: Ten years of observations on changes in geothermal surface Activity. In *Proceedings, the world geothermal congress* (pp. 19–24).

Olvera-García, E., Garduño-Monroy, V. H., Liotta, D., Brogi, A., Bermejo-Santoyo, G., & Guevara-Alday, J. A. (2020). Neogene-Quaternary normal and transfer faults controlling deep-seated geothermal systems: The case of San Agustín del Maíz (central Trans-Mexican Volcanic Belt, México). *Geothermics*, *86*, 101791. https://doi.org/10.1016/j.geothermics.2019.101791

Pandeli, E., Bertini, G., & Castellucci, P. (1991). The tectonic wedges complex of the Larderello area (southern Tuscany, Italy). *Bollettino della Societa Geologica Italiana*, *110*, 621–629.

Pandeli, E., Gianelli, G., Puxeddu, M., & Elter, F. M. (1994). The paleozoic basement of the northern Apennines: Stratigraphy, tectono-metamorphic evolution and alpine hydrothermal processes. *Memorie della Societa Geologica Italiana*, *48*, 627–654.

Panichi, C., Celati, R., Noto, P., Squarci, P., Taffi, L., & Tongiorgi, E. (1974). Oxygen and hydrogen isotope studies of the Larderello (Italy) geothermal field. In *Isotope techniques in groundwater hydrology* (Vol. SM182/27, pp. 3–28). I.A.E.A.

Panichi, C., & Tongiorgi, E. (1975). Carbon Isotopic composition of CO_2 from springs, fumaroles, Mofettes, and travertines of central and southern Italy: A preliminary prospection method of geothermal Area. In *Proceed. 2nd United Nations symposium on the development and use of geothermal resources* (Vol. 1, pp. 815–825).

Rahilly, K. E., & Fischer, T. P. (2021). Total diffuse CO_2 flux from Yellowstone caldera incorporating high CO_2 emissions from cold degassing sites. *Journal of Volcanology and Geothermal Research*, *419*, 107383. https://doi.org/10.1016/j.jvolgeores.2021.107383

Raich, J. W., & Schlesinger, W. H. (1992). The global carbon dioxide flux in soil respiration and its relationship to vegetation and climate. *Tellus*, *44B*(2), 81–99. https://doi.org/10.3402/tellusb.v44i2.15428

Rissmann, C., Christenson, B., Werner, C., Leybourne, M., Cole, J., & Gravley, D. (2012). Surface heat flow and CO_2 emissions within the Ohaaki hydrothermal field, Taupo Volcanic Zone, New Zealand. *Applied Geochemistry*, *27*(1), 223–239. https://doi.org/10.1016/j.apgeochem.2011.10.006

Rizzo, A. L., Pelorosso, B., Coltorti, M., Ntaflos, T., Bonadiman, C., Matusiak-Malek, M., et al. (2018). Geochemistry of noble gases and CO_2 in fluid inclusions from lithospheric mantle beneath Wilcza góra (Lower Silesia, Southwest Poland). *Frontiers of Earth Science*, *6*, 215. https://doi.org/10.3389/feart.2018.00215

Rochira, F., Caggianelli, A., & de Lorenzo, S. (2018). Regional thermo-rheological field related to granite emplacement in the upper crust: Implications for the Larderello area (Tuscany, Italy). *Geodinamica Acta*, *30*(1), 225–240. https://doi.org/10.1080/09853111.2018.1488912

Romagnoli, P., Arias, A., Barelli, A., Cei, M., & Casini, M. (2010). An updated numerical model of the Larderello–Travale geothermal system, Italy. *Geothermics*, *39*(4), 292–313. https://doi.org/10.1016/j.geothermics.2010.09.010

Rossello, E. A., & Gallardo, A. H. (2022). The Sierra Nevada de Santa Marta (Colombia) and Nevado de Famatina (Argentina): The effects of tectonic syntaxis on the topography of the Andes. *Journal of Structural Geology*, *160*, 104618. https://doi.org/10.1016/j.jsg.2022.104618

Rossetti, F., Faccenna, C., Jolivet, L., Goffé, B., & Funiciello, R. (2002). Structural signature and exhumation P–T–t paths of the blueschist units exposed in the interior of the Northern Apennine chain, tectonic implications. *Bollettino Società Geologica Italiana*, *1*, 829–842.

Rowland, J. V., & Sibson, R. H. (2004). Structural controls on hydrothermal flow in a segmented rift system, Taupo Volcanic Zone, New Zealand. *Geofluids*, *4*, 259–283. https://doi.org/10.1111/j.1468-8123.2004.00091.x

Sano, Y., & Marty, B. (1995). Origin of carbon in fumarolic gases from island arcs. *Chemical Geology*, *119*(1–4), 265–274. https://doi.org/10.1016/0009-2541(94)00097-r

Sbrana, A., Marianelli, P., Belgiorno, M., Sbrana, M., & Ciani, V. (2020). Natural CO_2 degassing in the Mount Amiata volcanic–geothermal area. *Journal of Volcanology and Geothermal Research*, *397*, 106852. https://doi.org/10.1016/j.jvolgeores.2020.106852

Scandiffio, G., Panichi, C., & Valenti, M. (1995). Geochemical evolution of fluids in the Larderello Geothermal field. In *Proceedings, the world geothermal congress 1995* (pp. 18–31).

Serri, G., Innocenti, F., & Manetti, P. (1993). Geochemical and petrological evidence of the subduction of delaminated adriatic continental lithosphere in the genesis of the Neogene–Quaternary magmatism of central Italy. *Tectonophysics*, *223*(1–2), 117–147. https://doi.org/10.1016/0040-1951(93)90161-c

Sharp, Z. D. (2017). Principles of stable isotope geochemistry (2nd ed.). https://doi.org/10.25844/h9q1-0p82

Sibson, R. H. (2000). Fluid involvement in normal faulting. In G. Cello & E. Tondi (Eds.), *The resolution of geological analysis and models for earthquake faulting studies* (Vol. 29, pp. 469–499).

Sillitoe, R., & Brogi, A. (2021). Geothermal systems in the northern Apennines, Italy: Modern analogues of Carlin-style gold deposits. *Economic Geology*, *116*(7), 1491–1501. https://doi.org/10.5382/econgeo.4883

Sinclair, A. J. (1974). Selection of threshold values in geochemical data using probability graphs. *Journal of Geochemical Exploration*, *3*(2), 129–149. https://doi.org/10.1016/0375-6742(74)90030-2

Smith, S. A. F., Holdsworth, R. E., & Collettini, R. E. (2011). Interactions between plutonism and low-angle normal faults in the upper crust: Insights from the Island of Elba. Italy. *Geological Society of America Bulletin*, *123*(1–2), 329–346. https://doi.org/10.1130/b30200.1

Spiess, R., Langone, A., Caggianelli, A., Stuart, F. M., Zucchi, M., Bianco, C., et al. (2021). Unveiling ductile deformation during fast exhumation of a granitic pluton in a transfer zone. *Journal of Structural Geology*, *147*, 104326. https://doi.org/10.1016/j.jsg.2021.104326

Tanelli, G. (1983). Mineralizzazioni metallifere e minerogenesi della Toscana. *Memorie della Societa Geologica Italiana*, *25*, 91–109.

Tassi, F., Cabassi, J., Calabrese, S., Nisi, B., Venturi, S., Capecchiacci, F., et al. (2016). Diffuse soil gas emissions of gaseous elemental mercury (GEM) from hydrothermal-volcanic systems: An innovative approach by using the static closed-chamber method. *Applied Geochemistry*, *66*, 234–241. https://doi.org/10.1016/j.apgeochem.2016.01.002

Tassi, F., Fiebig, J., Vaselli, O., & Nocentini, M. (2012). Origins of methane discharging from volcanic-hydrothermal, geothermal and cold emissions in Italy. *Chemical Geology*, *310–311*, 36–48. https://doi.org/10.1016/j.chemgeo.2012.03.018

Tassi, F., Vaselli, O., & Minissale, A. (1997). Geochemical monitoring for earthquake pecursors on two thermal springs and gases in the Siena Basin (northern Apennines, central Italy). *Journal of Earthquake Prediction Research*, *6*, 459–466.

Tassi, F., Venturi, S., Cabassi, J., Vaselli, O., Gelli, I., Cinti, D., & Capecchiacci, F. (2015). Biodegradation of CO_2, CH_4 and volatile organic compounds (VOCs) in soil gas from the Vicano–Cimino hydrothermal system (central Italy). *Organic Geochemistry*, *86*, 81–93. https://doi.org/10.1016/j.orggeochem.2015.06.004

Taussi, M., Brogi, A., Liotta, D., Nisi, B., Perrini, M., Vaselli, O., et al. (2022). CO_2 and heat energy transport by enhanced fracture permeability in the Monterotondo Marittimo-Sasso Pisano transfer fault system (Larderello Geothermal Field, Italy). *Geothermics*, *105*, 102531. https://doi.org/10.1016/j.geothermics.2022.102531

Taussi, M., Nisi, B., Brogi, A., Liotta, D., Zucchi, M., Venturi, S., et al. (2023). Dataset of the soil CO_2 degassing measurements and carbon isotopic composition of the interstitial gas in the Larderello geothermal system area, Italy. Version 1.0 [Dataset]. Interdisciplinary Earth Data Alliance (IEDA). https://doi.org/10.26022/IEDA/112908

Taussi, M., Nisi, B., Pizarro, M., Morata, D., Veloso, E. A., Volpi, G., et al. (2019). Sealing capacity of clay-cap units above the Cerro Pabellón hidden geothermal system (northern Chile) derived by soil CO_2 flux and temperature measurements. *Journal of Volcanology and Geothermal Research*, *384*, 1–14. https://doi.org/10.1016/j.jvolgeores.2019.07.009

Taussi, M., Nisi, B., Vaselli, O., Maza, S., Morata, D., & Renzulli, A. (2021). Soil CO_2 and temperature from a new geothermal area in the Cordón de Inacaliri volcanic complex (Northen Chile). *Geothermics*, *89*, 101961. https://doi.org/10.1016/j.geothermics.2020.101961

Vai, G. B., & Martini, I. P. (2001). *Anatomy of an orogen: The Apennines and adjacent Mediterranean basins* (p. 631). Kluwer Academic Publishers.

Van der Pluijm, B. A., & Marshak, S. (1996). *Earth structure* (2nd ed., p. 656). W.W. Norton & Company.

Varley, N. R., & Armienta, M. A. (2001). The absence of diffuse degassing at Popocatépetl volcano, Mexico. *Chemical Geology*, *177*(1–2), 157–173. https://doi.org/10.1016/s0009-2541(00)00389-2

Venturi, S., Tassi, F., Bicocchi, G., Cabassi, J., Capecchiacci, F., Capasso, G., et al. (2017). Fractionation processes affecting the stable carbon isotope signature of thermal waters from hydrothermal/volcanic systems: The examples of Campi Flegrei and Vulcano Island (southern Italy). *Journal of Volcanology and Geothermal Research*, *345*, 46–57. https://doi.org/10.1016/j.jvolgeores.2017.08.001

Venturi, S., Tassi, F., Magi, F., Cabassi, J., Ricci, A., Capecchiacci, F., et al. (2019). Carbon isotopic signature of interstitial soil gases reveals the potential role of ecosystems in mitigating geogenic greenhouse gas emissions: Case studies from hydrothermal systems in Italy. *Science of the Total Environment*, *655*, 887–898. https://doi.org/10.1016/j.scitotenv.2018.11.293

Viveiros, F., Cardellini, C., Ferreira, T., Caliro, S., Chiodini, G., & Silva, C. (2010). Soil CO_2 emissions at Furnas volcano, São Miguel Island, Azores archipelago: Volcano monitoring perspectives, geomorphologic studies, and land use planning application. *Journal of Geophysical Research*, *115*(B12), B12208. https://doi.org/10.1029/2010jb007555

Whiticar, M. J. (1999). Carbon and hydrogen isotope systematics of bacterial formation and oxidation of methane. *Chemical Geology*, *161*(1–3), 291–314. https://doi.org/10.1016/s0009-2541(99)00092-3

References From the Supporting Information

Lubenow, B. L., Fairley, J. P., Lindsey, C. R., & Larson, P. B. (2016). Influences on shallow ground temperatures in high flux thermal systems. *Journal of Volcanology and Geothermal Research*, *323*, 53–61. https://doi.org/10.1016/j.jvolgeores.2016.04.039